

Electronic Supplementary Information (ESI) for Chemical Science

Supporting Information

Spiro-Fluorene Locked Multi-Resonance Delayed Fluorescence Helical Framework: Efficient Circularly Polarized Electroluminescent Material

Xinliang Cai,^a Jinbei Wei,^{*,a} Zhiqiang Li,^b Yexuan Pu,^a Youwei Wu,^a and Yue Wang^{*,a}

^aState Key Laboratory of Supramolecular Structure and Materials, College of Chemistry, College of Electronic Science and Engineering, Jilin University, Changchun 130012, P. R. China.

E-mails: jinbwei@jlu.edu.cn and yuewang@jlu.edu.cn

^bJihua Laboratory, 28 Huandao Nan Road, Foshan, 528200, Guangdong Province, P. R. China.

Table of Contents

1. General Information	3
2. Theoretical calculation	4
3. Synthesis of Materials	4
4. Device Fabrication and Measurements	11
5. Calculation Formulas for the Photophysical Parameters	12
6. Supplementary Figures	13
7. Supplementary Tables	46
8. References	53

1. General Information

Thermo Fisher ITQ1100 GC/MS and Kratos AXIMA-CFR Kompact MALDI mass spectrometer were employed to measure the mass spectra. High resolution mass spectra (HRMS) were recorded on a Bruker Solarix FT-ICR mass spectrometer. Elemental analyses were performed on a flash EA 1112 spectrometer. Flash EA 1112 spectrometer was used to perform the elemental analyses. Bruker AVANCE III 500 MHz and 600 MHz were selected to measure the ¹H and ¹³C spectra with tetramethylsilane (TMS) as the internal standard. BOF-5-50 vacuum sublimation instrument (AnHui BEQ Equipment Technology CO., Ltd) was used to sublime the target compound. Shimadzu RF-5301 PC spectrometer and Shimadzu UV-2550 spectrophotometer were adopted to record the Photoluminescence (PL) emission spectra and UV-Vis absorption, respectively. The fluorescence and phosphorescent spectra taken at liquid nitrogen temperature (77 K) were recorded by Ocean Optics QE Pro with a 365 nm Ocean Optics LLS excitation source. Edinburgh FLS920 steady state fluorimeter equipping with an integrating sphere was employed to measure the absolute fluorescence quantum yields of both solutions and films at room temperature. FLS980 fluorescence lifetime measurement system with 365 nm LED excitation source was selected to investigate the transient PL decay and temperature-dependent transient PL decay of solid films. In the range of 30 to 800 °C, TA Q500 thermogravimeter was selected to perform the thermogravimetric analysis (TGA) of target molecules under nitrogen atmosphere at a heating rate of 10 K min⁻¹. BAS 100W Bioanalytical electrochemical work station was used to measure the electrochemical property with platinum disk as working electrode, platinum wire as auxiliary electrode, a porous glass wick Ag/Ag⁺ as pseudo reference electrode and ferrocene/ferrocenium as the internal standard. And 0.1 M solution of *n*-Bu₄NPF₆ which was the supporting electrolyte was utilized to measure the oxidation and reduction potentials (in anhydrous CH₂Cl₂ and DMF, respectively) at a scan rate of 100 mV s⁻¹. Pharmaron Beijing CO., LTD. was commissioned to accomplish the chiral separation of spiro-3TCzBN using Gilson 281 and a CHIRALPAK ID (30*250 mm, 5 μm) high performance liquid chromatogram (HPLC) column, with a mobile phase (propan-2-ol, IPA), under 13.0 ml min⁻¹ speed. And the chiral test of the residue samples (after thermal evaporation of the enantiomer under vacuum) using Shimadzu LC20ADXR, and a CHIRALPAK ID-3 (4.6*50 mm, 3

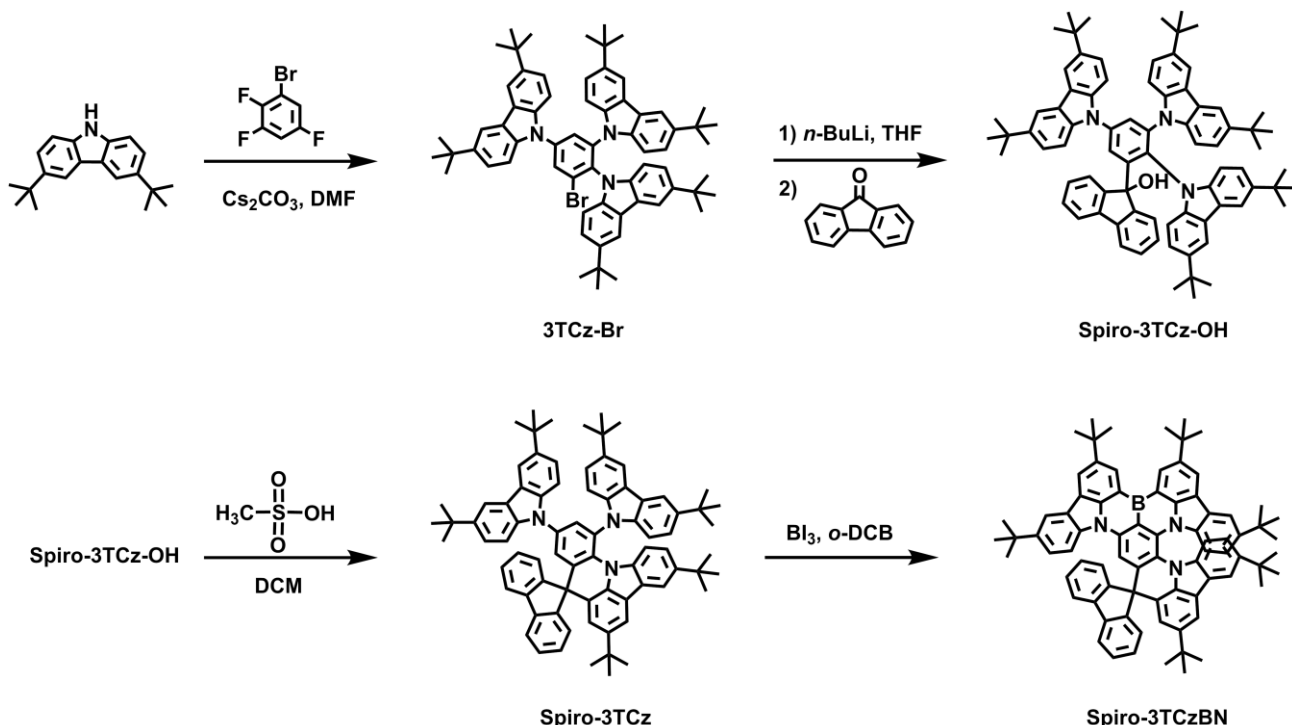
(μ m) HPLC column, with a mobile phase (IPA), under 0.5 ml min⁻¹ speed. Circular dichroism (CD) spectra were measured by a Jasco J-810 circular dichroism spectrometer with “Standard” sensitivity. The circularly polarized photoluminescence (CPL) and circularly polarized electroluminescence (CPEL) spectra were measured on a Jasco CPL-300 spectrophotometer with “Standard” sensitivity at scan speed of 100 nm min⁻¹ and respond time of 4.0 s employing “slit” mode.

2. Theoretical calculation

The structures were optimized using DFT (S_0 states) or TD-DFT (S_1 and T_1 states) methods by means of B3LYP with the 6-311G (d, p) basis set using Gaussian 09 software package.^[S1-S5] The HOMO/LUMO distributions are calculated on the basis of optimized S_0 state at the B3LYP/6-311G(d, p). All calculations were performed in the gas phase. The \hat{H}_{SOCs} were calculated by ORCA 4.2.1 software package by B3LYP method with TZVP basis set. The Natural transition orbital (NTO) analysis for the excited S_1 , T_1 and T_2 states are analyzed at B3LYP/6-311G (d, p) level and visualized with VMD 1.9.4. The RDG isosurface and RMSD was calculated by VMD 1.9.4.^[S6]

3. Synthesis of Materials

All reagents were purchased from *Energy Chemical Co.* and/or *J&K Scientific Ltd. Co.* and immediately used without further purification. Schlenk technology was strictly performed under nitrogen conditions in all reactions. Synthesis Procedure was showed below in detail.



Scheme S1. Synthetic procedures of Spiro-3TCzBN.

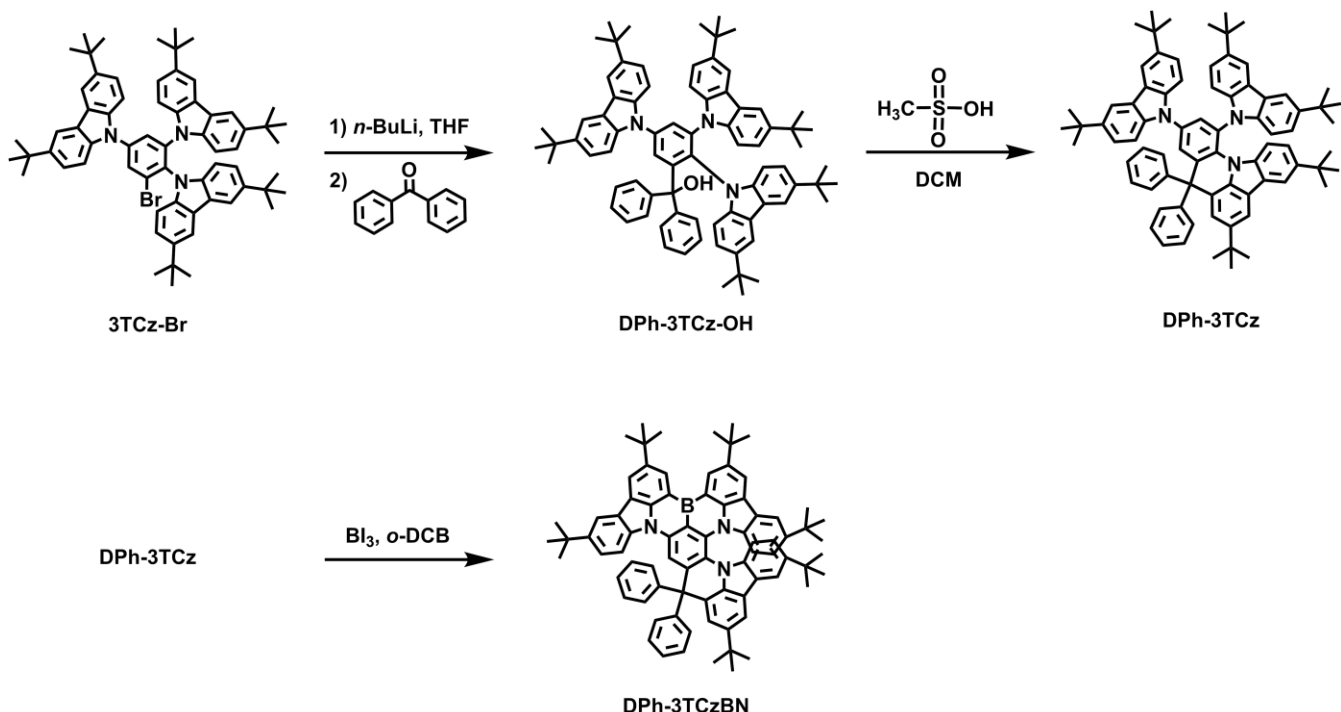
Synthesis of 3TCz-Br: 3,6-Di-*tert*-butylcarbazole (4.61 g, 16.5 mmol), Cs₂CO₃ (3.38 g, 16.5 mmol) and 1-bromo-2,3,5-trifluorobenzene (1.05 g, 5.0 mmol) were dissolved in *N,N*-dimethylformamide (DMF, 100 mL). The mixture was stirred at 150 °C for 12 h under nitrogen. After cooling to room temperature, the resulting product was diluted with chloroform and washed with water. The combined organic extracts were dried over Na₂SO₄ and concentrated under reduced pressure. The crude product was purified by column chromatography with dichloromethane/petroleum (1:7) as eluent to afford 3TCz-Br as a white solid (yield = 4.45 g, 90%). ¹H NMR (600 MHz, Methylene Chloride-*d*₂) δ 8.20 (d, *J* = 2.0 Hz, 2H), 7.72 (d, *J* = 8.6 Hz, 2H), 7.69 (d, *J* = 2.0 Hz, 2H), 7.66 (d, *J* = 1.9 Hz, 2H), 7.58 (dd, *J* = 8.7, 2.0 Hz, 2H), 7.07 (dd, *J* = 8.5, 2.0 Hz, 2H), 7.01 – 6.97 (m, 4H), 6.94 (d, *J* = 8.5 Hz, 2H), 1.48 (s, 18H), 1.35 (s, 18H), 1.32 (s, 18H). ¹³C NMR (151 MHz, Methylene Chloride-*d*₂) δ 145.42, 144.30, 144.18, 140.91, 140.28, 139.78, 139.72, 138.90, 134.27, 131.49, 128.56, 128.04, 125.45, 125.30, 124.74, 124.72, 124.04, 123.99, 117.90, 116.97, 116.82, 111.48, 110.65, 110.61, 36.01, 35.70, 35.67, 32.99, 32.94, 32.90. MALDI-TOF MS: m/z:987.44 [M]⁺ (calcd:987.51). Anal. Calcd for C₆₆H₇₄BrN₃: C, 80.13; H, 7.54; Br, 8.08; N, 4.25. Found: C, 80.18; H, 7.50; N, 4.27.

Synthesis of Spiro-3TCz-OH: The solution of *n*-butyllithium in hexane (1.8 mL, 2.50 M, 4.4 mmol) was added slowly to a solution of 3TCz-Br (3.96 g, 4.0 mmol) in anhydrous tetrahydrofuran (THF, 100 mL) at -78 °C under nitrogen atmosphere. After stirring at -78 °C for 4 h, the THF solution containing 9*H*-fluoren-9-one (0.72 g, 4.0 mmol) was added slowly to the mixture at 0 °C. After stirring at 30 °C for 24 h, the reaction mixture was cooled to room temperature. The resulted solution was extracted with dichloromethane/water, and the combined organic extracts were dried over Na₂SO₄ and concentrated by rotary evaporation. The crude product was purified by column chromatography with dichloromethane/petroleum (2: 1) as eluent to afford a white solid (2.36 g, 54%). ¹H NMR (600 MHz, Methylene Chloride-*d*₂) δ 9.16 (s, 1H), 8.23 (s, 2H), 7.88 (s, 1H), 7.84 (d, *J* = 8.6 Hz, 2H), 7.63 (dd, *J* = 8.6, 2.2 Hz, 2H), 7.60 (s, 2H), 7.33 (d, *J* = 7.3 Hz, 2H), 7.29 (s, 2H), 6.99 (q, *J* = 8.6 Hz, 4H), 6.85 (t, *J* = 7.3 Hz, 2H), 6.81 (t, *J* = 7.3 Hz, 2H), 6.69 (d, *J* = 7.3 Hz, 2H), 6.63 (d, *J* = 8.6 Hz, 2H), 6.23 (s, 2H), 1.50 (s, 18H), 1.27 (s, 18H), 1.23 (s, 18H). ¹³C NMR (151 MHz, Methylene Chloride-*d*₂) δ 148.79, 145.06, 143.49, 140.92, 140.76, 140.37, 139.97, 132.92, 129.67, 128.85, 128.71, 128.22, 125.39, 125.24, 125.00, 124.04, 123.68, 123.49, 122.78, 120.63, 117.82, 116.53, 115.45, 111.86, 111.45, 110.83, 83.54, 36.01, 35.56, 35.43, 33.04, 32.97, 32.84, 32.38. MALDI: m/z: 1089.53 [M]⁺ (calcd:1089.65). Anal. Calcd for C₇₉H₈₃N₃O: C, 87.01; H, 7.67; N, 3.85; O, 1.47. Found: C, 87.03; H, 7.64; N, 3.85.

Synthesis of Spiro-3TCz: The methanesulfonic acid (0.77 g, 8.0 mmol) was added slowly to a solution of 3TCz-OH (2.18 g, 2.0 mmol) in anhydrous dichloromethane (DCM, 100 mL) at 0 °C. After stirring at 30 °C for 3 h, the reaction mixture was cooled to room temperature. The resulted solution was extracted with dichloromethane/water, and the combined organic extracts were dried over Na₂SO₄ and concentrated by rotary evaporation. The crude product was purified by column chromatography with dichloromethane/petroleum (1: 6) as eluent to afford a white solid (2.08 g, 97%). ¹H NMR (600 MHz, Methylene Chloride-*d*₂) δ 8.02 (d, *J* = 2.0 Hz, 2H), 8.00 (d, *J* = 2.0 Hz, 2H), 7.90 (s, 1H), 7.83 (d, *J* = 7.8 Hz, 2H), 7.72 (d, *J* = 2.0 Hz, 1H), 7.63 (d, *J* = 2.4 Hz, 1H), 7.43 (td, *J* = 7.5, 1.1 Hz, 2H), 7.38 (d, *J* = 7.6 Hz, 2H), 7.35 (dd, *J* = 8.7, 2.0 Hz, 2H), 7.31–7.28 (m, 4H), 7.14 (d, *J* = 8.7 Hz, 2H), 7.10 (d, *J* = 8.6 Hz, 2H), 6.91 (d, *J* = 2.5 Hz, 1H), 6.68 (d, *J* = 1.6 Hz, 1H), 6.52 (d, *J* = 8.8 Hz, 1H), 6.40 (dd, *J* = 8.8, 2.0 Hz, 1H), 1.40 (s, 18H), 1.39 (s, 18H), 1.25 (s, 9H), 1.18 (s, 9H). ¹³C NMR (151 MHz, Methylene Chloride-*d*₂) δ 155.58, 147.93,

144.41, 144.30, 141.07, 140.10, 139.88, 138.23, 137.63, 134.48, 129.65, 129.47, 128.18, 127.36, 126.92, 126.60, 126.25, 125.40, 125.13, 125.00, 124.95, 124.82, 124.51, 123.79, 121.78, 120.76, 117.49, 117.42, 116.69, 116.19, 114.14, 110.33, 110.21, 59.77, 36.16, 35.84, 35.48, 32.97, 32.89, 32.57. MALDI: m/z: 1071.66 [M]+ (calcd:1071.64). Anal. Calcd for C₇₉H₈₁N₃: C, 88.47; H, 7.61; N, 3.92. Found: C, 88.42; H, 7.63; N, 3.92.

Synthesis of Spiro-3TCzBN: To a solution of spiro-3TCz (1.07 g, 1.0 mmol) in *o*-dichlorobenzene was slowly added Bi₃ (392 mg, 1 mmol) in pressure flask at room temperature under nitrogen protection. After sealing tube and stirring for 20 h under 120 °C, the mixture was cooled to 0 °C. Then the reaction mixture was carefully quenched by addition of (1.29 g, 10 mmol) *N,N*-diisopropylethylamine (DIPEA). The product was extracted with dichloromethane, and the combined organic layer was dried over anhydrous Na₂SO₄. After filtration and evaporation, the crude product was purified by column chromatography with dichloromethane/petroleum (1: 7) as eluent to afford a orange solid (0.41 g, 36%). ¹H NMR (600 MHz, Methylene Chloride-*d*₂) δ 9.07 (s, 1H), 9.00 (s, 1H), 8.48 (s, 1H), 8.36 (s, 1H), 8.10 (s, 1H), 8.05 (d, *J* = 7.9 Hz, 1H), 7.93 (d, *J* = 5.0 Hz, 3H), 7.83 (s, 1H), 7.54 (t, *J* = 7.6 Hz, 1H), 7.47 (d, *J* = 7.7 Hz, 1H), 7.34 (t, *J* = 7.5 Hz, 1H), 7.31 (s, 1H), 7.23 (t, *J* = 7.4 Hz, 1H), 7.19 (d, *J* = 8.4 Hz, 1H), 7.15 (t, *J* = 7.4 Hz, 1H), 7.05 (d, *J* = 7.5 Hz, 1H), 6.92 (d, *J* = 8.7 Hz, 1H), 6.81 (t, *J* = 7.9 Hz, 2H), 6.67 (s, 1H), 6.63 (d, *J* = 8.8 Hz, 1H), 6.07 (d, *J* = 8.7 Hz, 1H), 1.65 (s, 9H), 1.56 (s, 9H), 1.38 (s, 9H), 1.20 (s, 9H), 1.18 (s, 9H), 1.15 (s, 9H). ¹³C NMR (151 MHz, Methylene Chloride-*d*₂) δ 158.00, 156.32, 146.00, 145.41, 145.31, 144.85, 144.82, 142.93, 141.93, 140.32, 139.28, 138.85, 138.34, 137.89, 137.49, 137.43, 135.93, 135.34, 131.37, 130.11, 129.34, 128.94, 128.69, 128.53, 128.42, 128.16, 128.12, 126.64, 126.14, 125.91, 125.08, 124.31, 124.10, 123.93, 123.66, 123.24, 123.11, 122.44, 121.61, 121.23, 121.01, 120.59, 120.47, 117.73, 117.47, 116.19, 116.06, 115.15, 113.09, 112.18, 110.98, 109.37, 58.76, 35.35, 35.21, 34.99, 34.72, 34.56, 34.43, 32.14, 32.01, 31.77, 31.62, 31.57, 31.50. HRMS (MALDI-FTICR): m/z: 1079.6280 [M]+ (calcd:1079.6296). Anal. Calcd for C₇₉H₇₈BN₃: C, 87.83; H, 7.28; B, 1.00; N, 3.89. Found: C, 87.83; H, 7.32; N, 3.92.



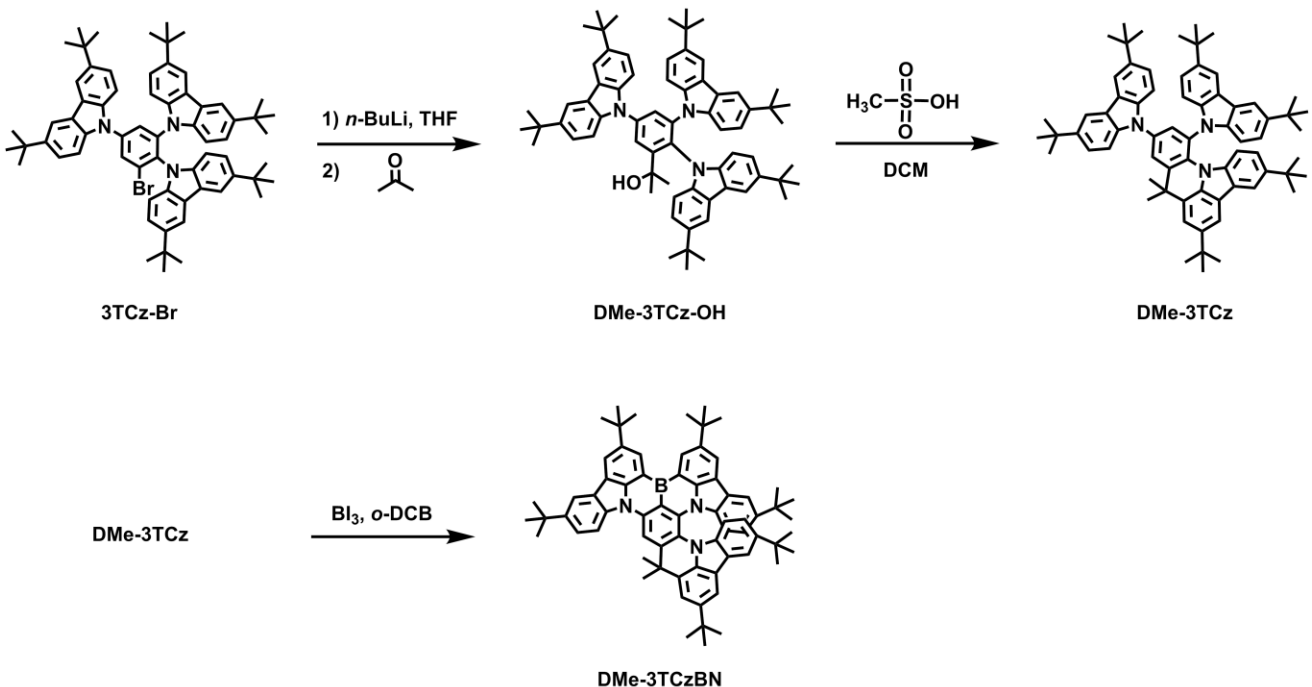
Scheme S2. Synthetic procedures of DPh-3TCzBN.

Synthesis of DPh-3TCz-OH: DPh-3TCz-OH was synthesized by replacing 9*H*-fluoren-9-one with benzophenone according to the synthetic procedure of Spiro-3TCz-OH. The crude product was purified by column chromatography with dichloromethane/petroleum (2: 1) as eluent to afford a white solid (58% yield). ¹H NMR (600 MHz, Methylene Chloride-*d*₂) δ 8.10 (d, *J* = 1.9 Hz, 2H), 7.78 (d, *J* = 2.5 Hz, 1H), 7.62 (d, *J* = 1.8 Hz, 2H), 7.58 (d, *J* = 2.5 Hz, 1H), 7.53 (d, *J* = 1.9 Hz, 2H), 7.40 (dd, *J* = 8.7, 2.0 Hz, 2H), 7.37 – 7.31 (m, 12H), 7.00 (dd, *J* = 8.6, 1.8 Hz, 2H), 6.91 (dd, *J* = 8.6, 1.8 Hz, 2H), 6.81 (d, *J* = 8.6 Hz, 2H), 6.69 (d, *J* = 8.6 Hz, 2H), 1.43 (s, 18H), 1.28 (s, 18H), 1.26 (s, 18H). ¹³C NMR (151 MHz, Methylene Chloride-*d*₂) δ 151.67, 147.22, 145.17, 144.35, 143.46, 142.04, 141.24, 140.74, 139.49, 139.39, 135.29, 130.60, 129.48, 129.29, 129.00, 128.67, 125.18, 125.15, 124.89, 124.05, 124.01, 123.54, 117.68, 116.51, 116.28, 112.91, 111.27, 110.62, 85.26, 35.92, 35.60, 32.93, 32.86. MALDI: m/z: 1091.44 [M]⁺ (calcd:1091.67). Anal. Calcd for C₇₉H₈₅N₃O: C, 86.85; H, 7.84; N, 3.85; O, 1.46. Found: C, 86.72; H, 7.82; N, 3.83.

Synthesis of DPh-3TCz: DPh-3TCz was synthesized according to the synthetic procedure of Spiro-3TCz. The crude product was purified by column chromatography with dichloromethane/petroleum (1: 6) as eluent to afford a white solid (94% yield). ¹H NMR (600

MHz, Methylene Chloride-*d*₂) δ 8.09 (d, *J* = 2.0 Hz, 2H), 7.92 (d, *J* = 2.1 Hz, 3H), 7.70 (d, *J* = 2.4 Hz, 1H), 7.58 (d, *J* = 1.9 Hz, 1H), 7.46 – 7.42 (m, 3H), 7.31 (t, *J* = 7.9 Hz, 6H), 7.26 (d, *J* = 7.1 Hz, 2H), 7.25 – 7.22 (m, 6H), 7.15 (d, *J* = 1.5 Hz, 1H), 6.92 (d, *J* = 8.6 Hz, 2H), 6.32 (d, *J* = 8.7 Hz, 1H), 6.21 (dd, *J* = 8.7, 2.0 Hz, 1H), 1.43 (s, 18H), 1.42 (s, 9H), 1.37 (s, 18H), 1.11 (s, 9H). ¹³C NMR (151 MHz, Methylene Chloride-*d*₂) δ 147.54, 146.94, 145.17, 144.38, 144.20, 140.43, 140.11, 140.05, 139.20, 134.11, 133.15, 131.50, 129.88, 129.28, 128.38, 128.12, 127.65, 127.45, 126.97, 125.22, 124.95, 124.80, 124.25, 123.51, 117.57, 117.23, 116.33, 115.89, 114.12, 110.48, 109.91, 60.25, 36.34, 35.90, 35.81, 35.40, 33.05, 33.01, 32.98, 32.50. MALDI: m/z: 1073.54 [M]⁺ (calcd:1073.66). Anal. Calcd for C₇₉H₈₃N₃: C, 88.30; H, 7.79; N, 3.91. Found: C, 88.32; H, 7.73; N, 3.90.

Synthesis of DPh-3TCzBN: DPh-3TCzBN was synthesized according to the synthetic procedure of Spiro-3TCzBN. The crude product was purified by column chromatography with dichloromethane/petroleum (1: 7) as eluent to afford a white solid (32% yield). ¹H NMR (500 MHz, Chloroform-*d*) δ 9.17 (s, 2H), 8.46 (s, 2H), 8.20 (s, 1H), 7.96 (s, 4H), 7.58 – 7.25 (m, 14H), 7.19 (t, *J* = 7.4 Hz, 1H), 6.68 (s, 2H), 1.74 (s, 9H), 1.68 (s, 9H), 1.49 (s, 9H), 1.46 (s, 9H), 1.21 (s, 18H). ¹³C NMR (126 MHz, Chloroform-*d*) δ 144.91, 137.91, 130.81, 129.80, 128.24, 128.04, 126.64, 126.54, 124.97, 123.68, 121.17, 116.91, 35.32, 34.70, 32.31, 32.04. HRMS (MALDI-FTICR): m/z: 1081.6436 [M]⁺ (calcd:1081.6452). Anal. Calcd for C₇₉H₈₀BN₃: C, 87.67; H, 7.45; B, 1.00; N, 3.88. Found: C, 87.72; H, 7.42; N, 3.90.



Scheme S3. Synthetic procedures of DMe-3TCzBN.

Synthesis of DMe-3TCz-OH: DMe-3TCz-OH was synthesized by replacing 9*H*-fluoren-9-one with acetone according to the synthetic procedure of Spiro-3TCz-OH. The crude product was purified by column chromatography with dichloromethane/petroleum (2: 1) as eluent to afford a white solid (50% yield). ^1H NMR (600 MHz, Methylene Chloride-*d*₂) δ 8.46 (d, *J* = 2.4 Hz, 1H), 8.19 (d, *J* = 1.8 Hz, 2H), 7.75 (d, *J* = 2.4 Hz, 1H), 7.67 (d, *J* = 8.6 Hz, 2H), 7.63 (dd, *J* = 6.6, 1.9 Hz, 4H), 7.56 (dd, *J* = 8.7, 1.8 Hz, 2H), 7.15 (dd, *J* = 8.5, 1.9 Hz, 2H), 7.03 (td, *J* = 6.8, 3.4 Hz, 4H), 6.86 (d, *J* = 8.6 Hz, 2H), 1.53 (s, 6H), 1.47 (s, 18H), 1.30 (s, 18H), 1.29 (s, 18H). ^{13}C NMR (151 MHz, Methylene Chloride-*d*₂) δ 143.72, 142.60, 142.03, 140.30, 139.57, 138.58, 127.78, 126.07, 124.04, 123.83, 123.18, 122.74, 122.60, 122.21, 116.48, 115.33, 115.16, 111.46, 110.05, 109.33, 73.56, 34.68, 34.37, 34.30, 31.75, 31.69, 31.63, 31.55. MALDI: m/z: 967.74 [M]⁺ (calcd: 967.64). Anal. Calcd for C₆₉H₈₁N₃O: C, 85.58; H, 8.43; N, 4.34; O, 1.65. Found: C, 85.52; H, 8.42; N, 4.33.

Synthesis of DMe-3TCz: DMe-3TCz was synthesized according to the synthetic procedure of Spiro-3TCz. The crude product was purified by column chromatography with dichloromethane/petroleum (1: 6) as eluent to afford a white solid (94% yield). ^1H NMR (600 MHz, Methylene Chloride-*d*₂) δ 8.17 (d, *J* = 2.0 Hz, 2H), 7.95 (d, *J* = 1.9 Hz, 2H), 7.93 (d, *J* = 2.4 Hz, 1H), 7.87 (d, *J* = 1.6 Hz, 1H), 7.67 (d, *J* = 2.4 Hz, 1H), 7.63 (d, *J* = 2.0 Hz, 1H), 7.59 (d, *J* = 1.6 Hz,

1H), 7.51 (dd, J = 8.7, 1.9 Hz, 2H), 7.47 (d, J = 8.6 Hz, 2H), 7.21 (dd, J = 8.6, 2.0 Hz, 2H), 6.93 (d, J = 8.5 Hz, 2H), 6.41 (d, J = 8.7 Hz, 1H), 6.28 (dd, J = 8.7, 2.0 Hz, 1H), 1.84 (s, 6H), 1.52 (s, 9H), 1.46 (s, 18H), 1.36 (s, 18H), 1.14 (s, 9H). ^{13}C NMR (151 MHz, Methylene Chloride- d_2) (151 MHz, Methylene Chloride- d_2) δ 147.73, 144.88, 144.30, 144.23, 142.21, 140.54, 140.03, 138.10, 137.91, 134.59, 132.53, 129.85, 127.44, 126.83, 126.80, 125.31, 125.24, 125.12, 124.80, 124.56, 124.32, 123.38, 119.49, 117.66, 117.30, 116.33, 115.23, 114.02, 110.51, 110.19, 40.21, 36.48, 35.94, 35.80, 35.41, 33.20, 33.05, 32.96, 32.54, 32.29. MALDI: m/z: 949.72 [M]⁺ (calcd:949.63). Anal. Calcd for C₆₀H₇₉N₃: C, 87.20; H, 8.38; N, 4.42. Found: C, 87.12; H, 8.33; N, 4.20.

Synthesis of DMe-3TCzBN: DMe-3TCzBN was synthesized according to the synthetic procedure of Spiro-3TCzBN. The crude product was purified by column chromatography with dichloromethane/petroleum (1: 7) as eluent to afford a white solid (26% yield). ^1H NMR (500 MHz, Chloroform- d) δ 9.18 (s, 2H), 8.78–8.16 (m, 5H), 7.93 (s, 7H), 6.70 (s, 2H), 2.19 (s, 3H), 2.08 (s, 3H), 1.74 (s, 9H), 1.70 (s, 9H), 1.60 (s, 9H), 1.56 (s, 9H), 1.21 (s, 18H). ^{13}C NMR (126 MHz, Chloroform- d) δ 146.07, 139.37, 129.92, 125.30, 121.58, 115.89, 113.78, 35.22, 34.49, 32.18, 31.97. HRMS (MALDI-FTICR): m/z: 957.6128 [M]⁺ (calcd:957.6138). Anal. Calcd for C₆₉H₇₆BN₃: C, 86.49; H, 8.00; B, 1.13; N, 4.39. Found: C, 86.52; H, 8.02; N, 4.30.

4. Device Fabrication and Measurements

The indium tin oxide (ITO) glass substrates with a sheet resistance of 15 Ω per square were cleaned with optical detergent, deionized water, acetone and isopropanol successively, and then treated with plasma for 5 minutes. Subsequently, they were transferred to a vacuum chamber. Under high vacuum ($< 8 \times 10^{-5}$ Pa), the organic materials were deposited onto the ITO glass substrates at a rate of 1.0 \AA s^{-1} . After finishing the deposition of organic layers, ITO glass substrates were patterned by a shadow mask with an array of 2.0 mm \times 2.5 mm openings. Then Liq and Al were successively deposited at a rate of 0.1 and 5.0 \AA s^{-1} , respectively. The EL spectrum, CIE coordinate and luminance intensity of the OLEDs were recorded by Photo Research PR655, meanwhile, the current density (J) and driving voltage (V) were recorded by Keithley 2400. By assuming Lambertian distribution, the external quantum efficiency (EQE) was estimated according to brightness, electroluminescence spectrum and current density. When

assuming the external emission profile is Lambertian distribution, the EQE can be determined by the following equations:

$$\text{EQE} = \frac{N_p}{N_e} \quad (\text{S1})$$

$$N_p = \frac{\int L_e(\lambda) \cdot W(\lambda) \cdot d\lambda}{h \times c} \times \pi \times D \quad (\text{S2})$$

$$N_e = \frac{I}{e} \quad (\text{S3})$$

Where N_p is the photons number, N_e is the electrons number, $L_e(\lambda)$ is the spectral radiance ($\text{W sr}^{-1} \text{ m}^{-2} \text{ nm}^{-1}$), $W(\lambda)$ is the wavelength, $d\lambda=1$, D is the emitting area, h is the Planck's constant, c is the speed of light in vacuum, e is the elementary charge of electron and I is the injected current.

5. Calculation Formulas for the Photophysical Parameters:

The calculation of the kinetic parameters assumes that internal conversion process of the singlet exciton is the main nonradiative decay.^[S7-S9]

$$k_r = \Phi_F k_F + \Phi_{TADF} k_{TADF} \quad (\text{S6})$$

$$k_{nr} = k_r (1 - \Phi_{PL}) / \Phi_{PL} \quad (\text{S7})$$

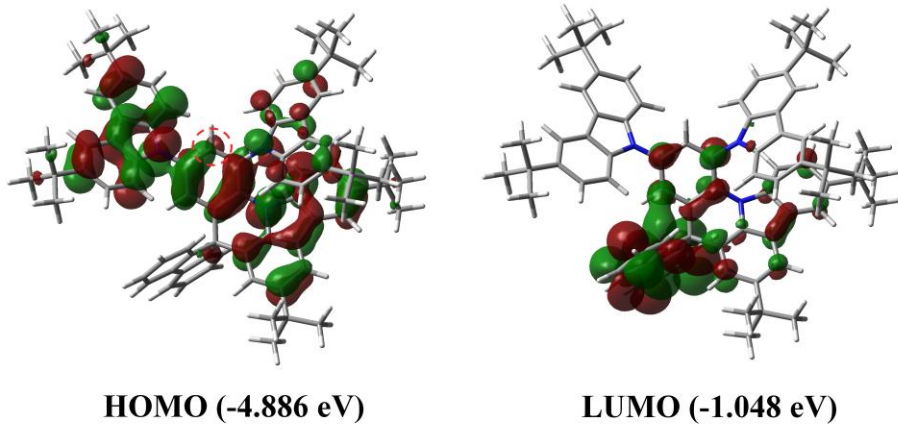
$$k_{ISC} = k_F - k_r - k_{nr} \quad (\text{S8})$$

$$k_{RISC} = (k_F k_{TADF} \Phi_{TADF}) / (k_{ISC} \Phi_F) \quad (\text{S9})$$

Where k_F and k_{TADF} represent the decay rate constants for prompt and delayed fluorescence, respectively, which are in reciprocal relationship with the decay time constants (τ_F and τ_{TADF}) experimentally determined from transient PL characteristics; Φ_{PL} is the total fluorescence quantum yield, Φ_F is the prompt fluorescent component of Φ_{PL} , Φ_{TADF} is the delayed fluorescent component of Φ_{PL} . k_r , k_{nr} , k_{ISC} and k_{RISC} are rate constants of radiative decay, non-radiative decay, intersystem crossing and reverse intersystem crossing, respectively.

6. Supplementary Figures

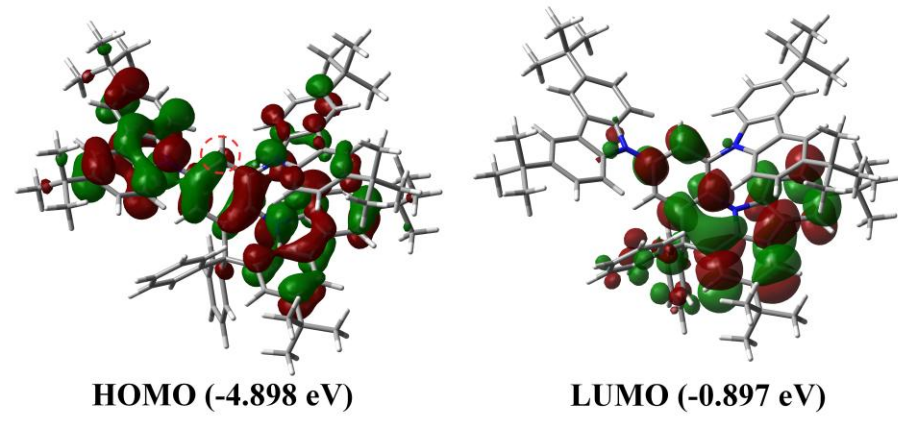
a)



HOMO (-4.886 eV)

LUMO (-1.048 eV)

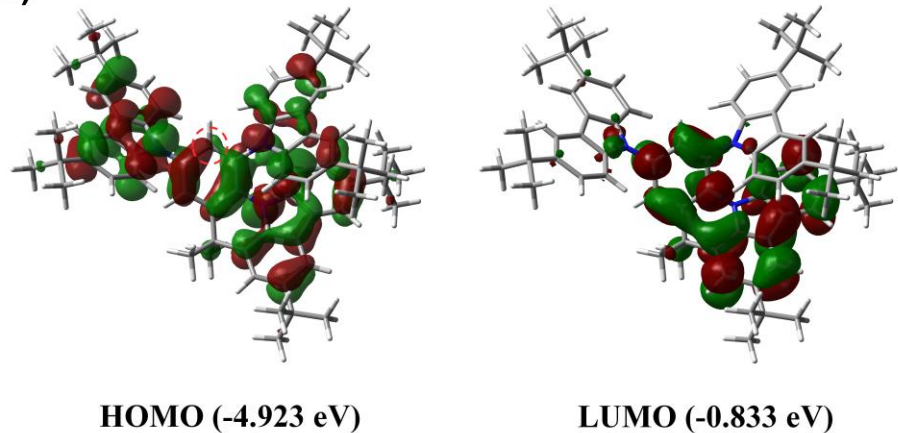
b)



HOMO (-4.898 eV)

LUMO (-0.897 eV)

c)



HOMO (-4.923 eV)

LUMO (-0.833 eV)

Figure S1. Highest occupied molecular orbitals (HOMOs) and lowest unoccupied molecular orbitals (LUMOs) of a) Spiro-3TCz, b) DPh-3TCz and c) DMe-3TCz calculated at the B3LYP/6-311G(d, p) level of theory.

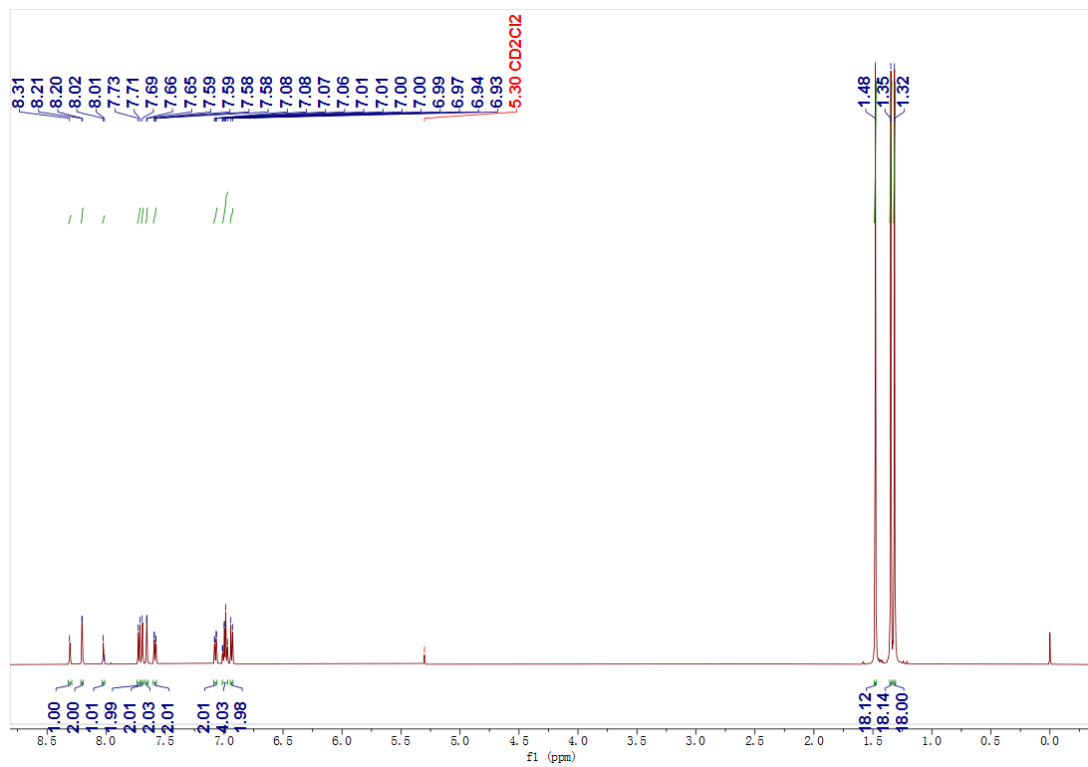


Figure S2. ^1H NMR spectrum of 3TCz-Br (600 MHz, Methylene Chloride- d_2).

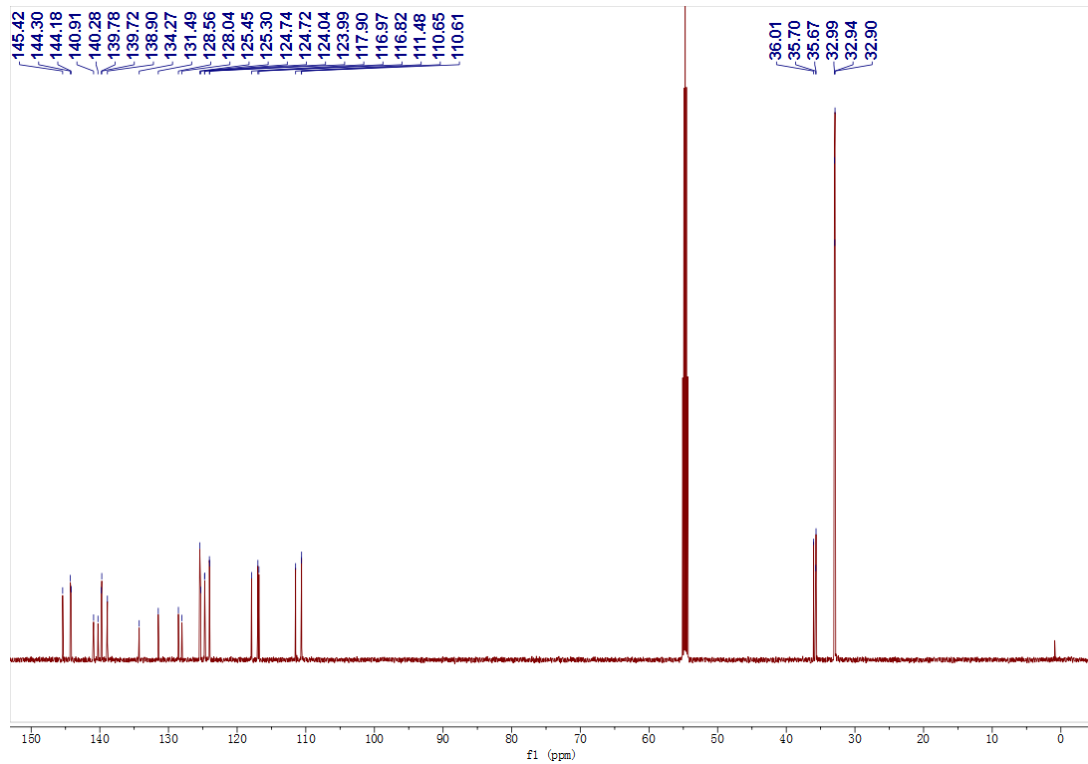


Figure S3. ^{13}C NMR spectrum of 3TCz-Br (151 MHz, Methylene Chloride- d_2).

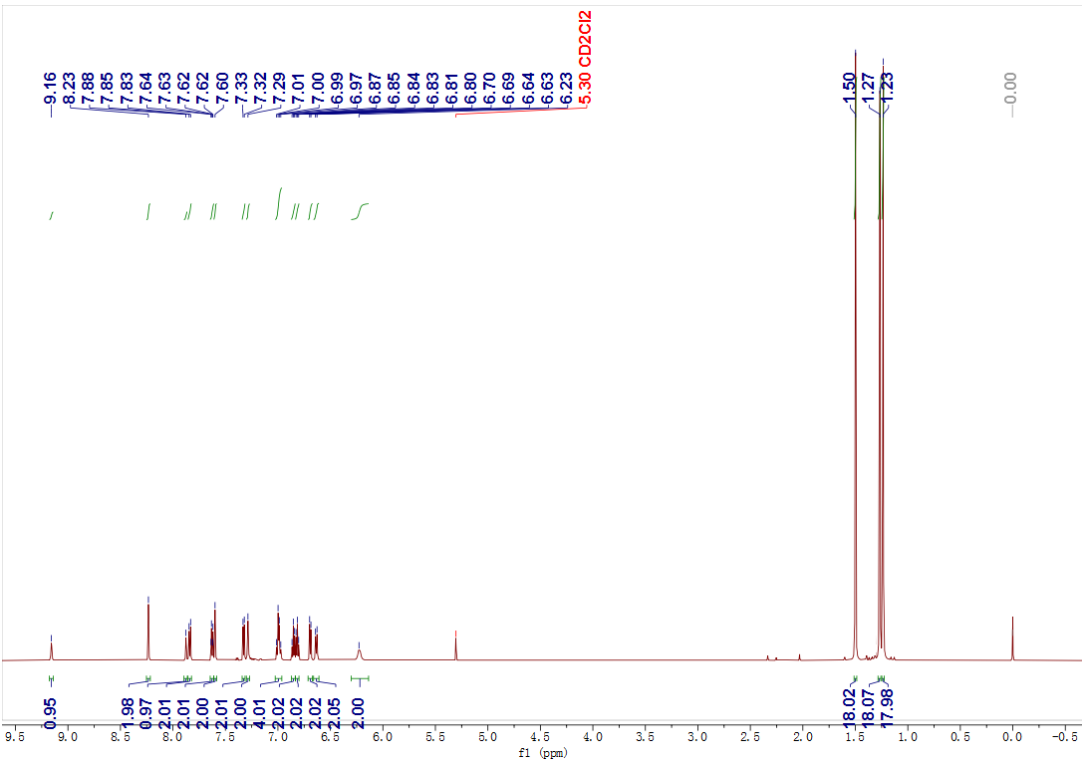


Figure S4. ^1H NMR spectrum of Spiro-3TCz-OH (600 MHz, Methylene Chloride- d_2).

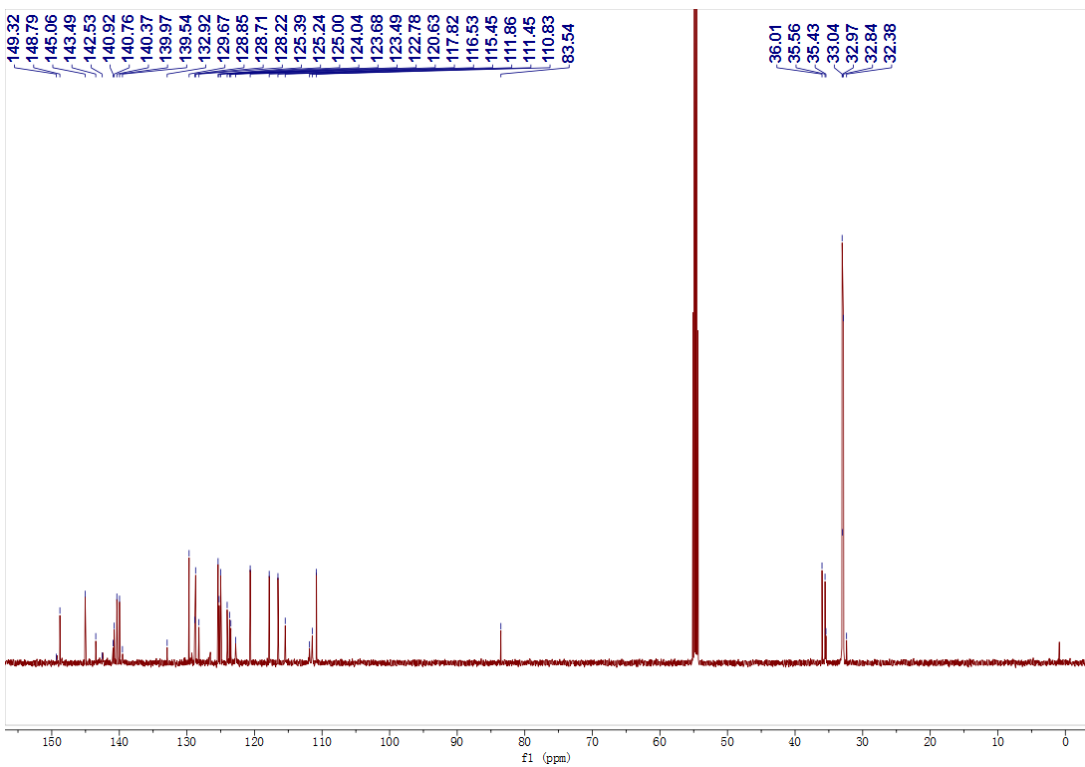


Figure S5. ^{13}C NMR spectrum of Spiro-3TCz-OH (151 MHz, Methylene Chloride- d_2).

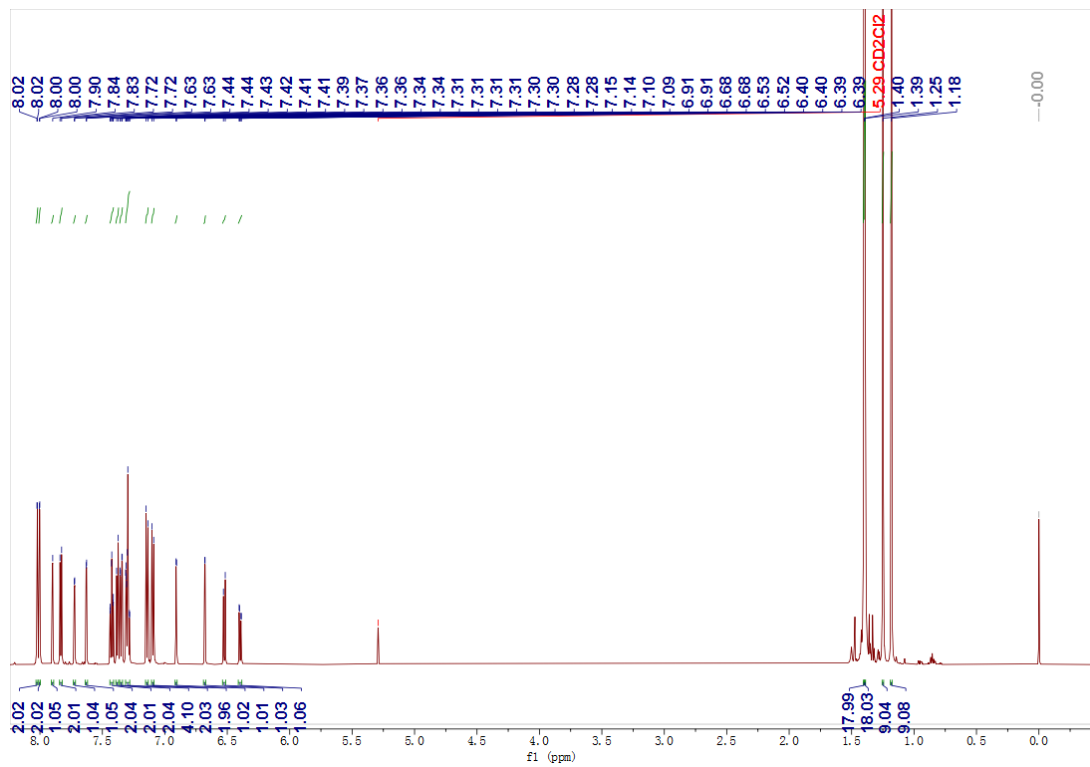


Figure S6. ^1H NMR spectrum of Spiro-3TCz (600 MHz, Methylene Chloride- d_2).

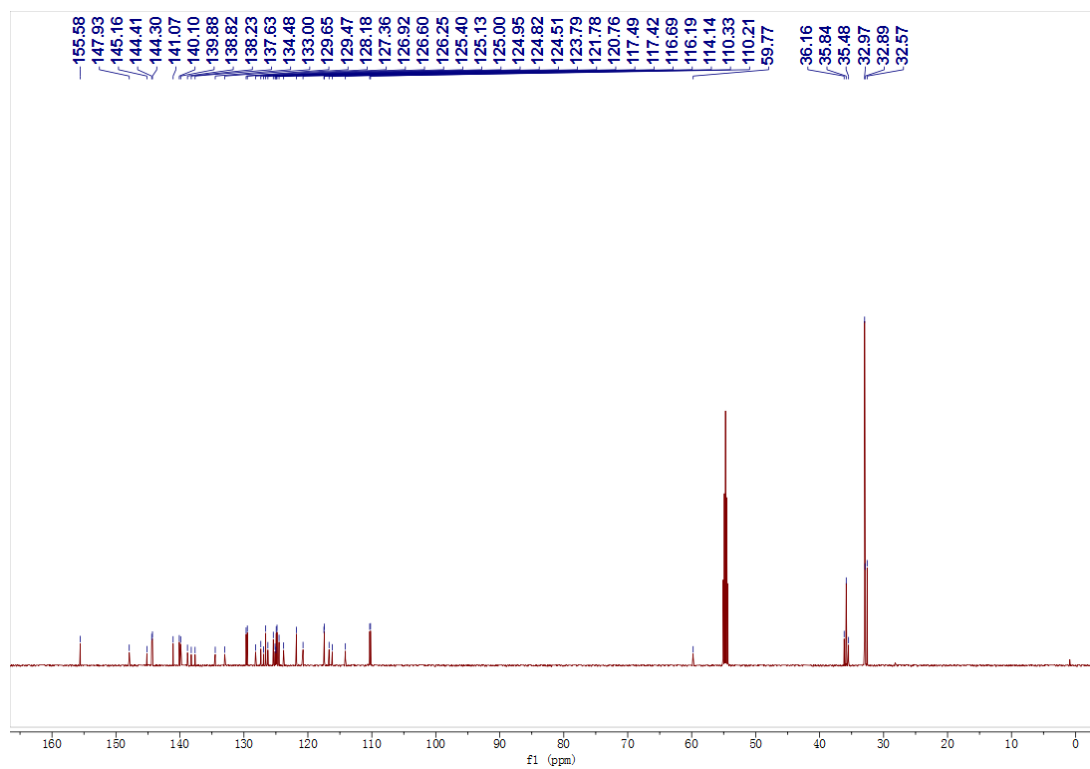


Figure S7. ^{13}C NMR spectrum of Spiro-3TCz (151 MHz, Methylene Chloride- d_2).

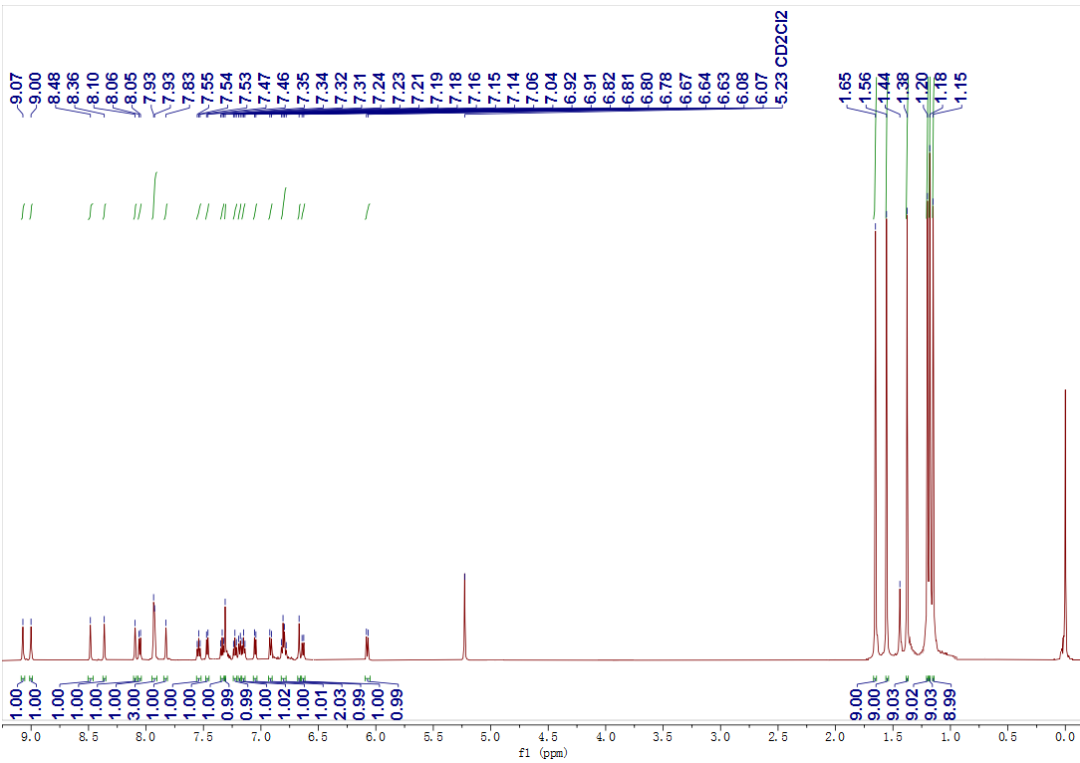


Figure S8. ^1H NMR spectrum of Spiro-3TCzBN (600 MHz, Methylene Chloride- d_2).

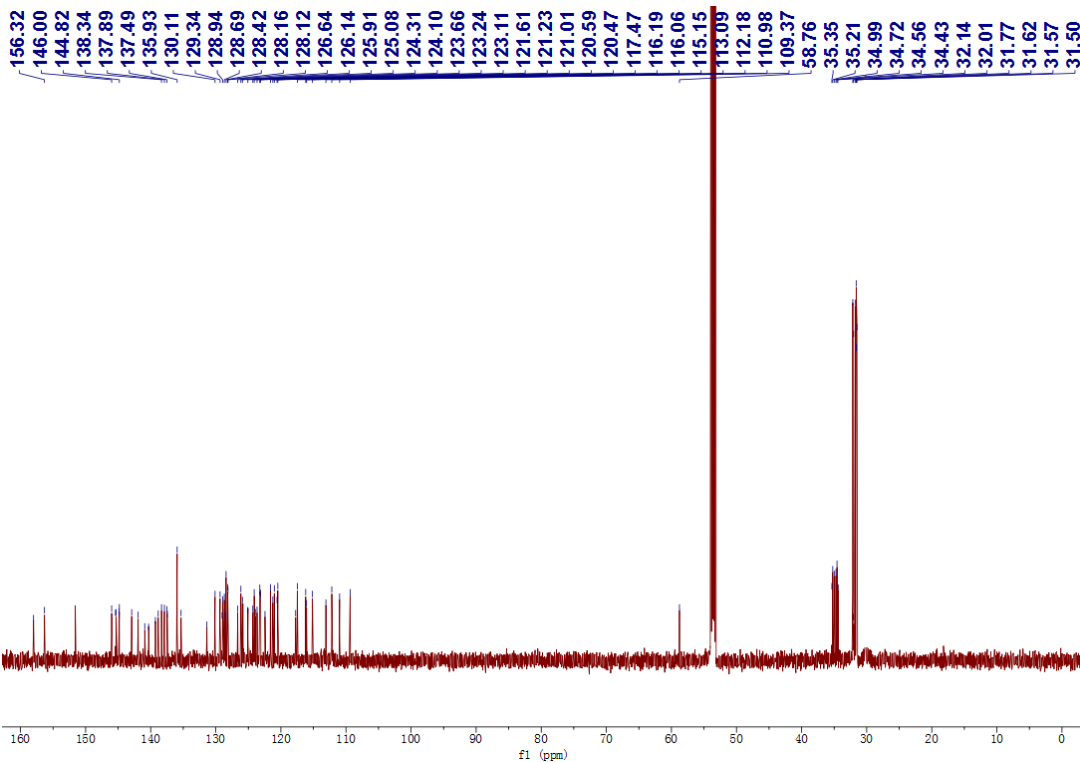


Figure S9. ^{13}C NMR spectrum of Spiro-3TCzBN (151 MHz, Methylene Chloride- d_2).

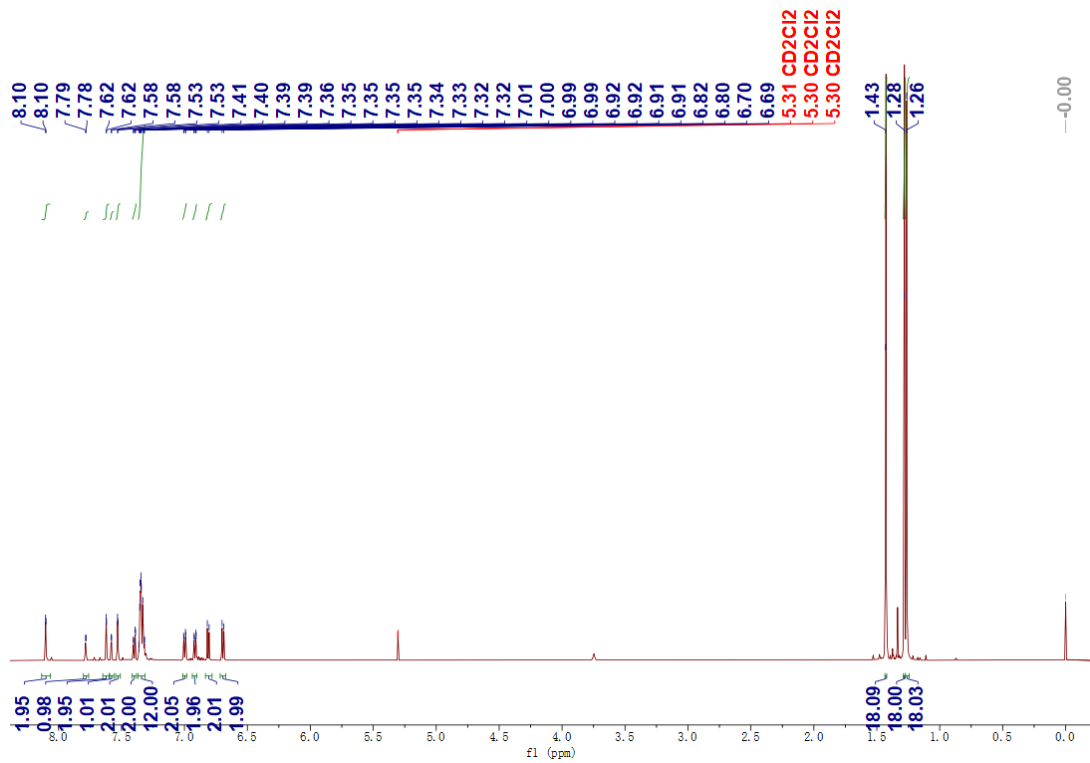


Figure S10. ^1H NMR spectrum of DPh-3TCz-OH (600 MHz, Methylene Chloride- d_2).

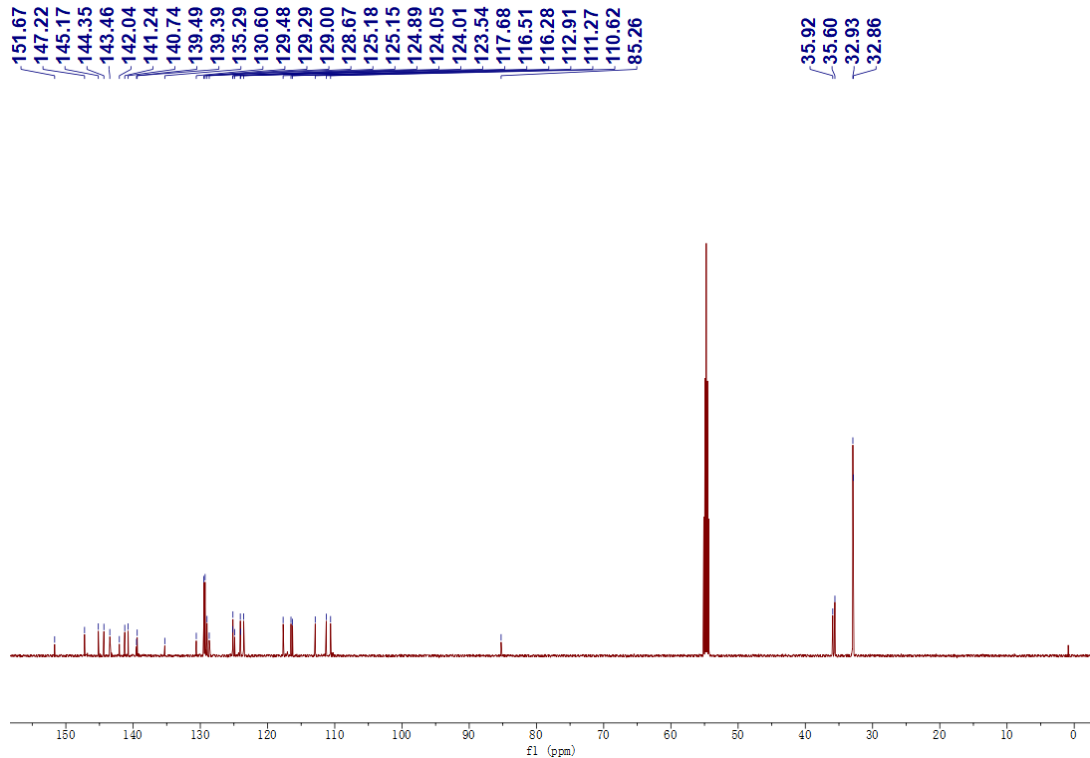


Figure S11. ^{13}C NMR spectrum of DPh-3TCz-OH (151 MHz, Methylene Chloride- d_2).

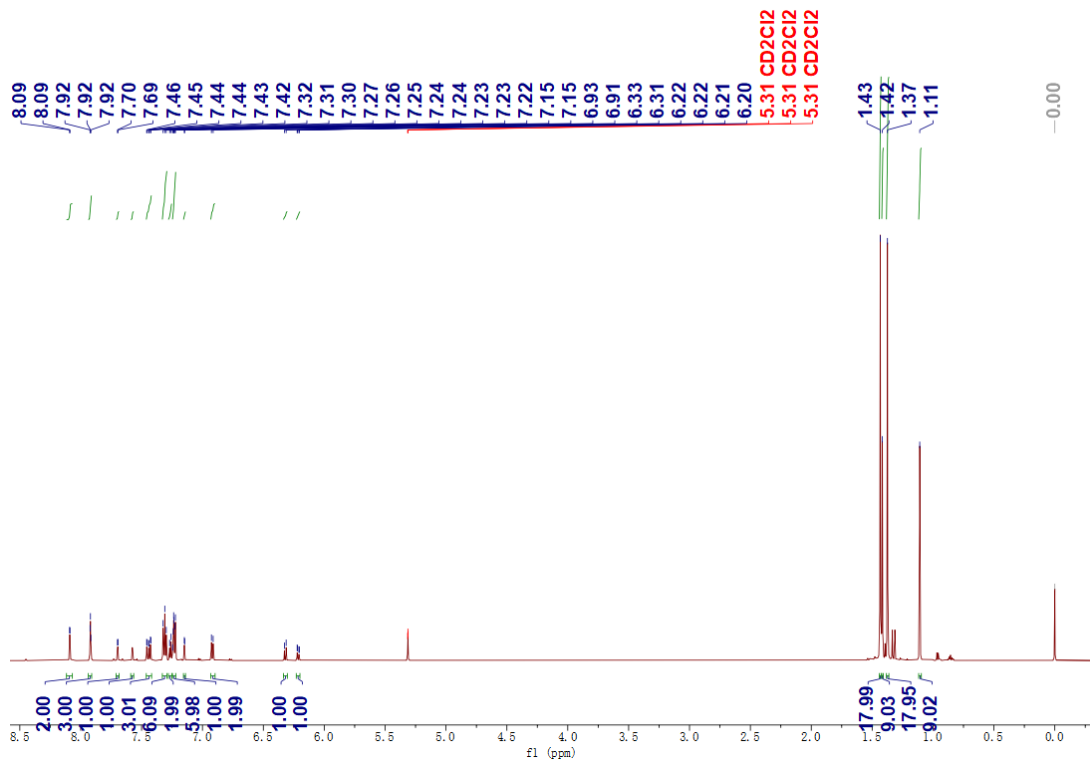


Figure S12. ^1H NMR spectrum of DPh-3TCz (600 MHz, Methylene Chloride- d_2).

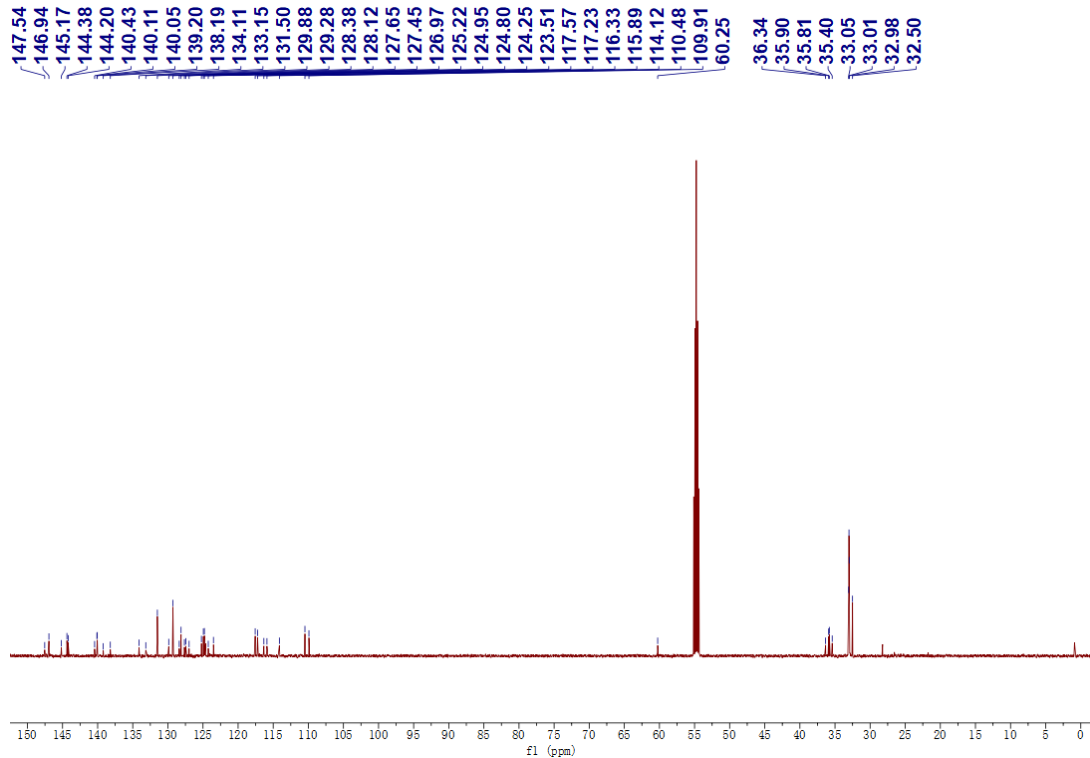


Figure S13. ^{13}C NMR spectrum of DPh-3TCz (151 MHz, Methylene Chloride- d_2).

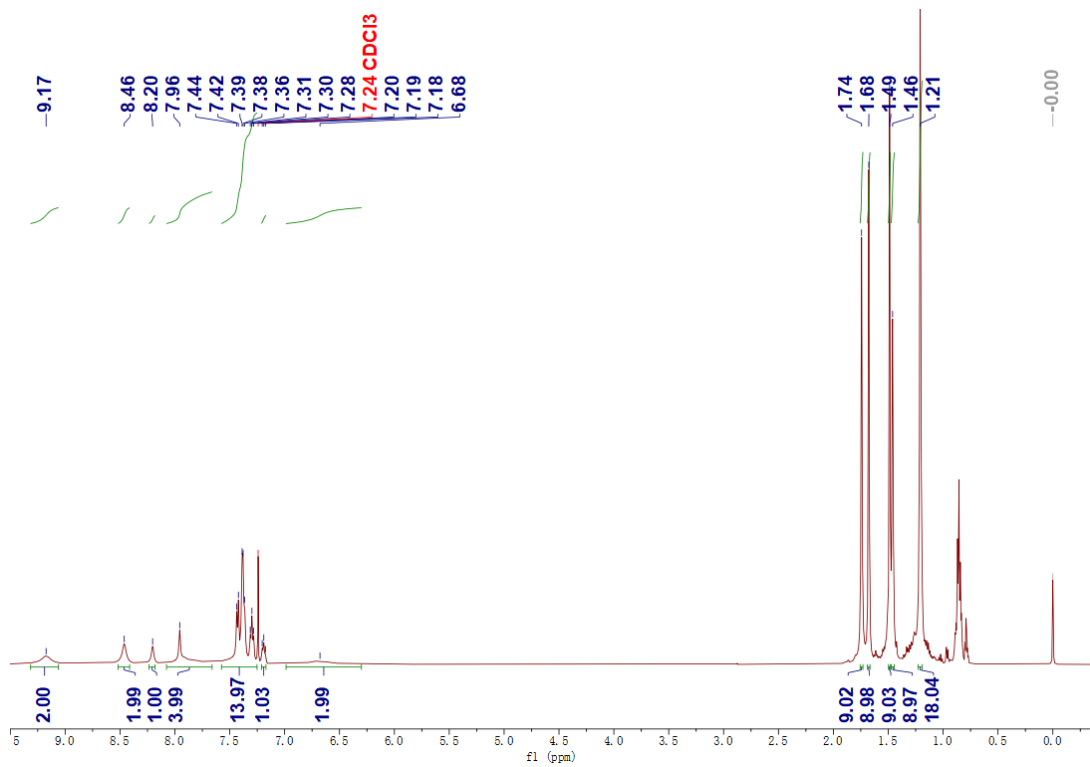


Figure S14. ^1H NMR spectrum of DPh-3TCzBN (500 MHz, Chloroform-*d*).

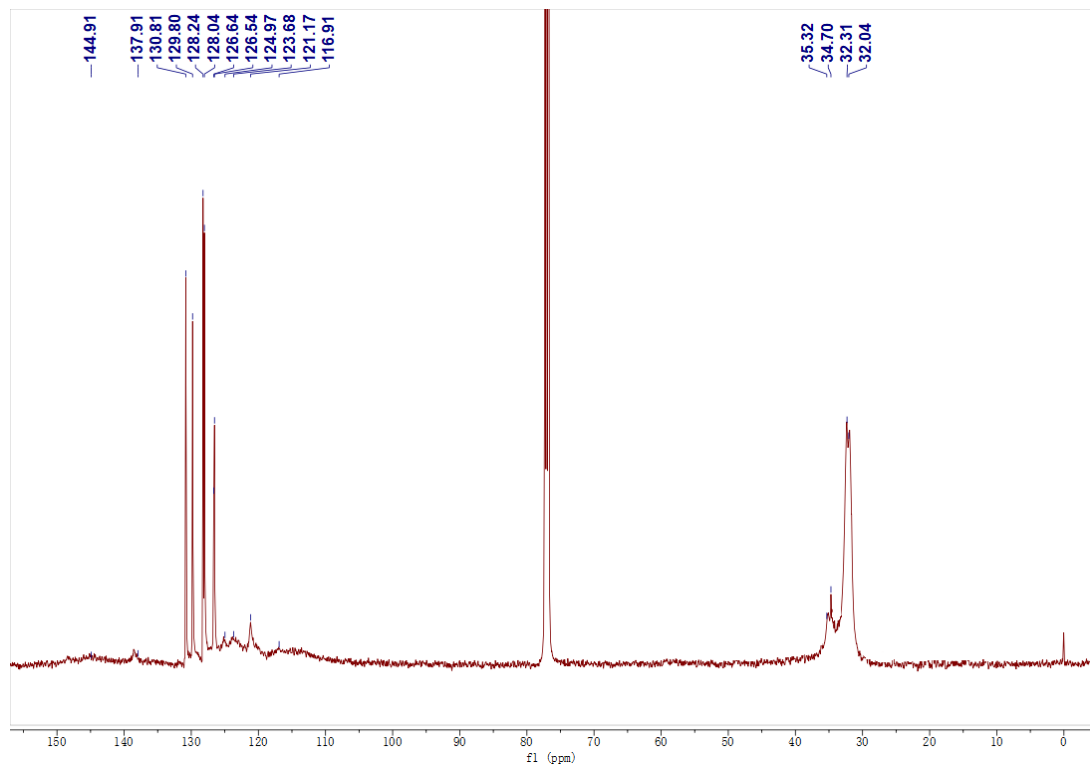


Figure S15. ^{13}C NMR spectrum of DPh-3TCzBN (126 MHz, Chloroform-*d*).

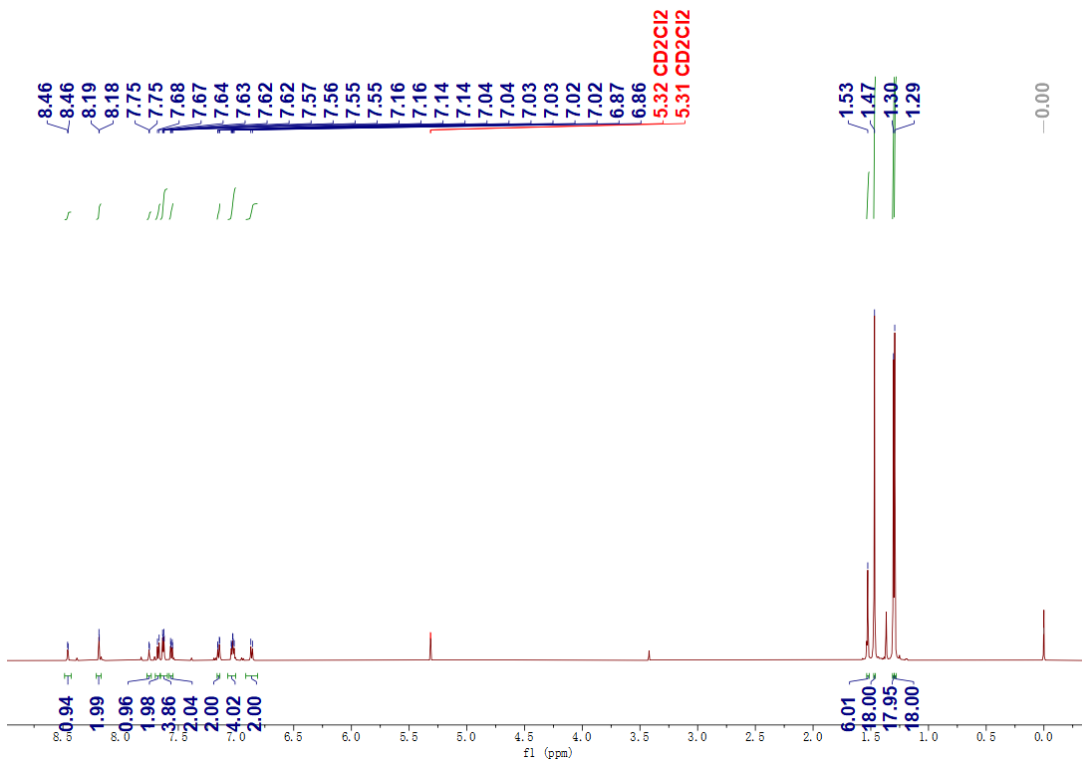


Figure S16. ^1H NMR spectrum of DMe-3TCz-OH (600 MHz, Methylene Chloride- d_2).

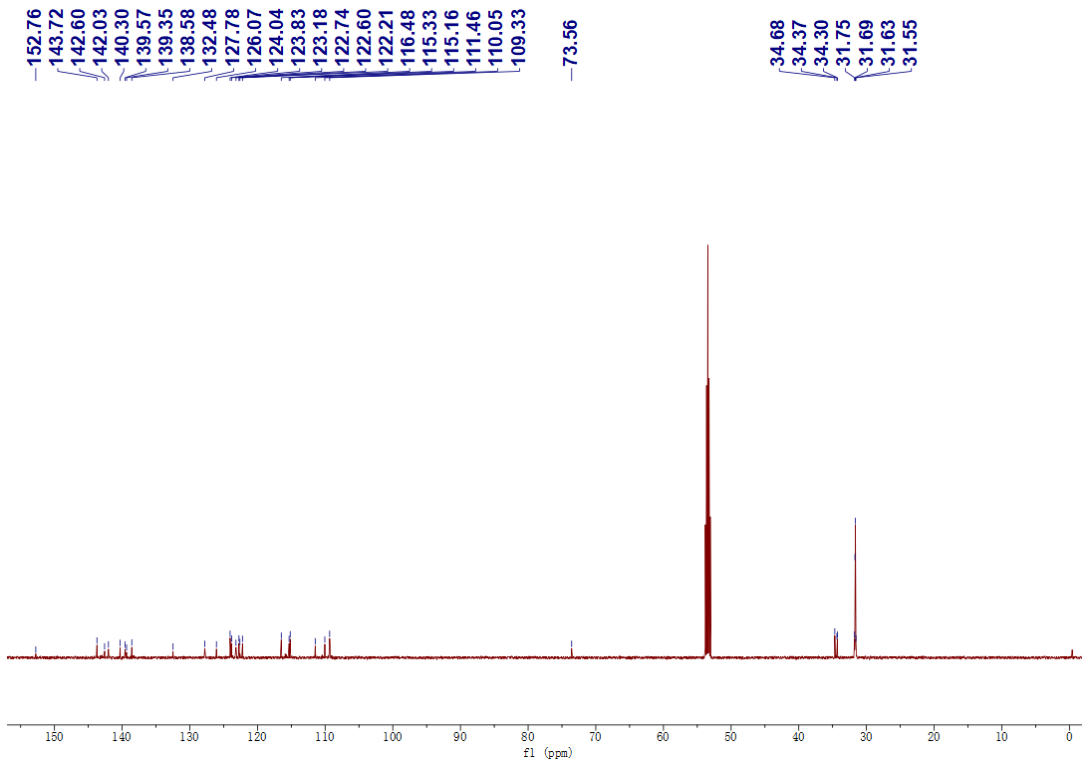


Figure S17. ^{13}C NMR spectrum of DMe-3TCz-OH (600 MHz, Methylene Chloride- d_2).

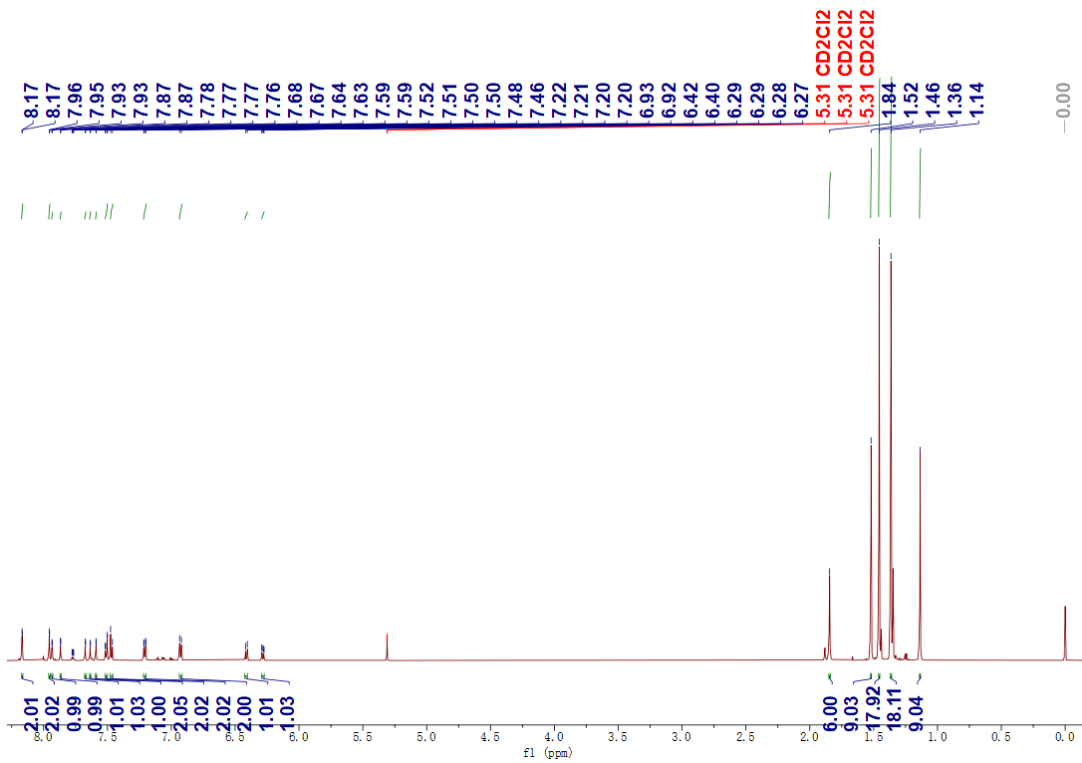


Figure S18. ^1H NMR spectrum of DMe-3TCz (600 MHz, Methylene Chloride- d_2).

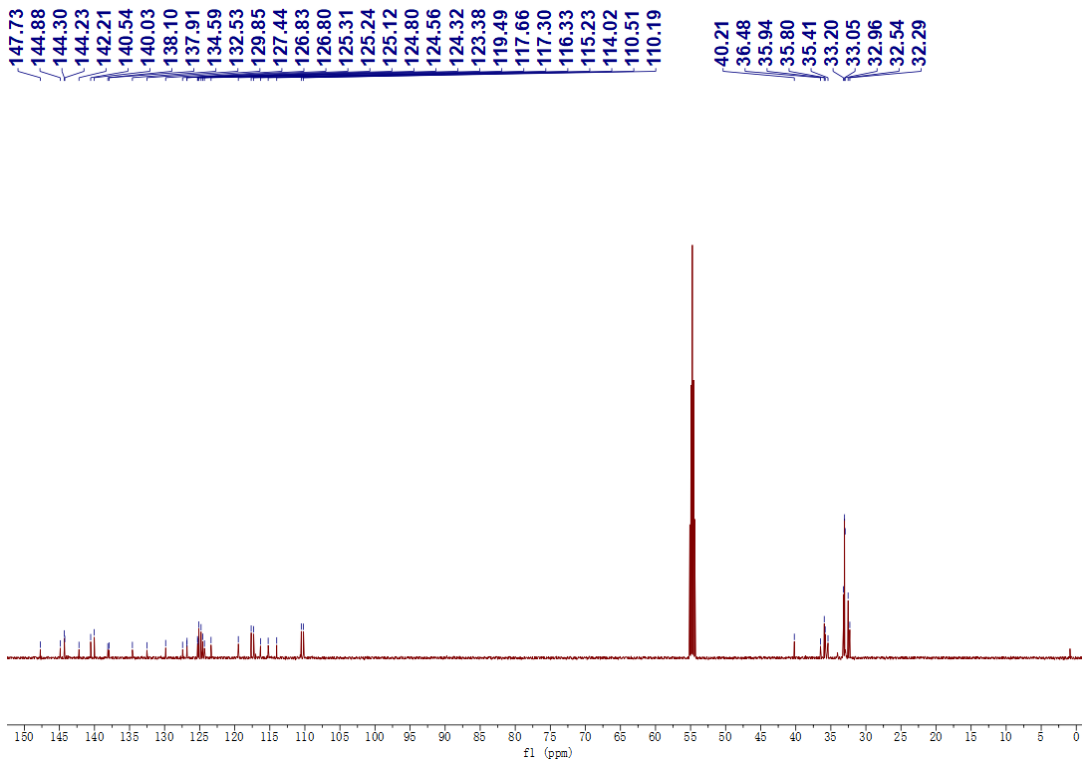


Figure S19. ^{13}C NMR spectrum of DMe-3TCz (600 MHz, Methylene Chloride- d_2).

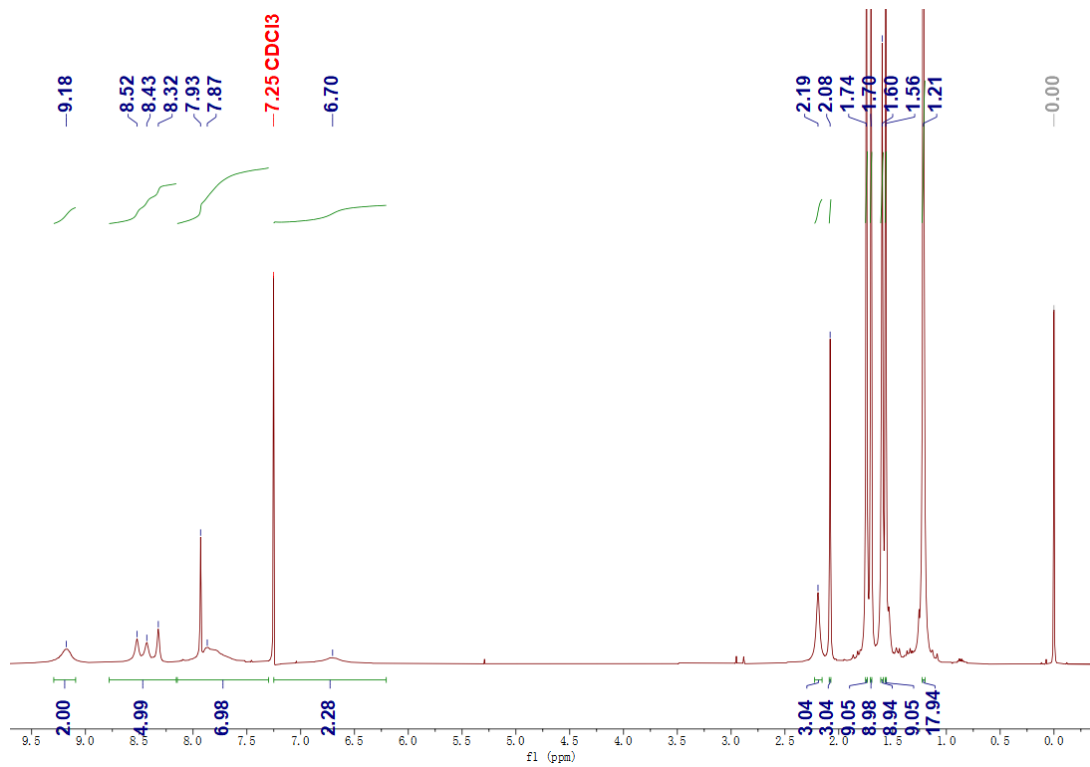


Figure S20. ^1H NMR spectrum of DMe-3TCzBN (500 MHz, Chloroform-*d*).

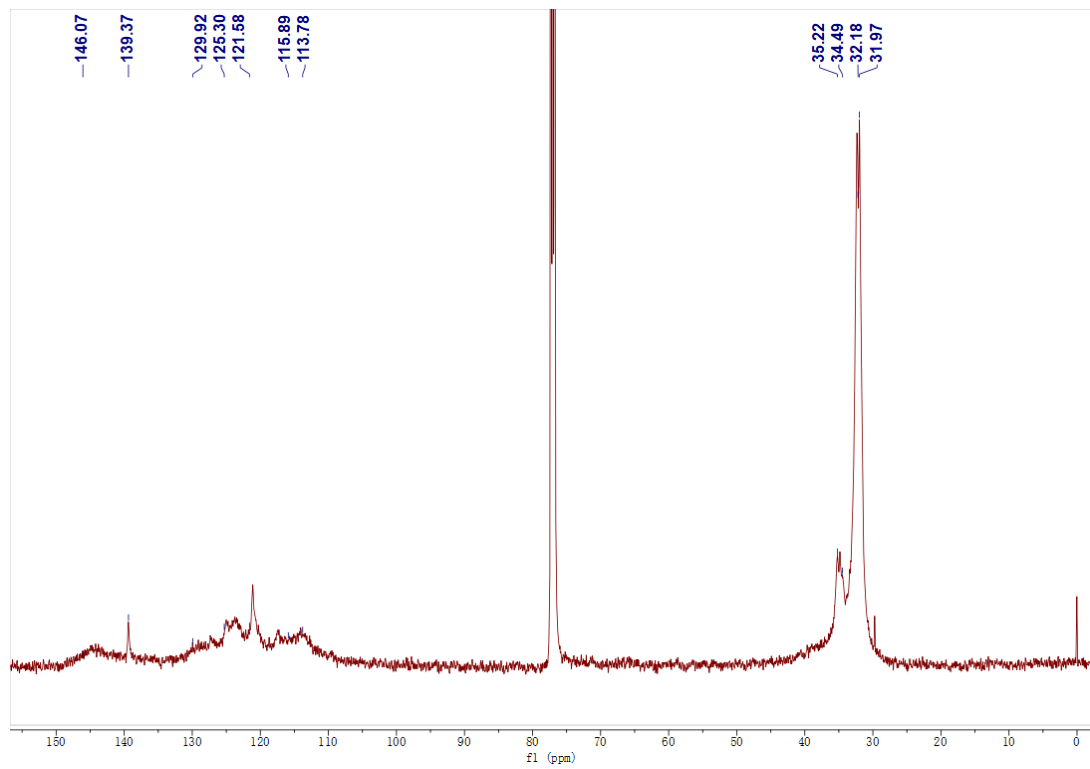


Figure S21. ^{13}C NMR spectrum of DMe-3TCzBN (126 MHz, Chloroform-*d*).

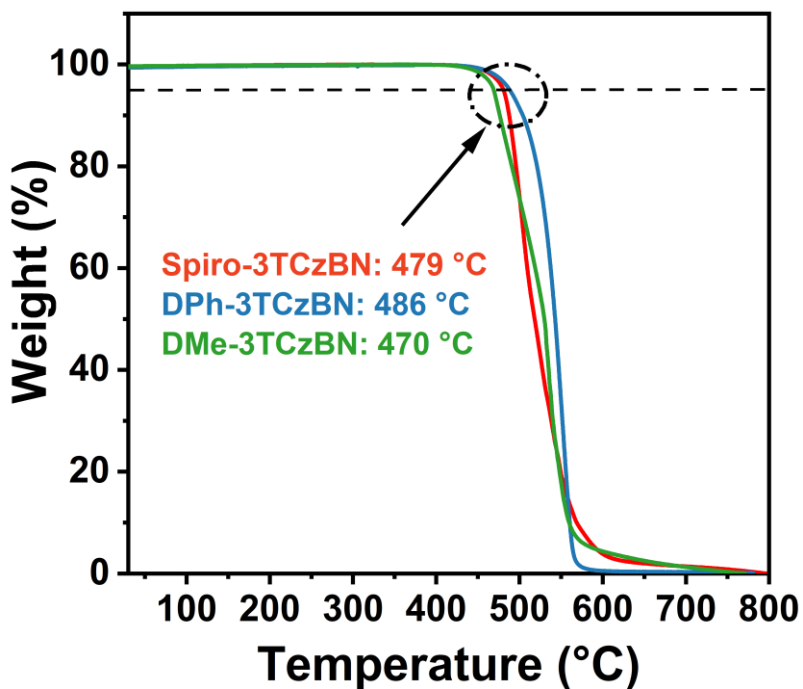


Figure S22. TGA curves of Spiro-3TCzBN, DPh-3TCzBN and DMe-3TCzBN at a scanning rate of 10 $^{\circ}\text{C min}^{-1}$ under N_2 .

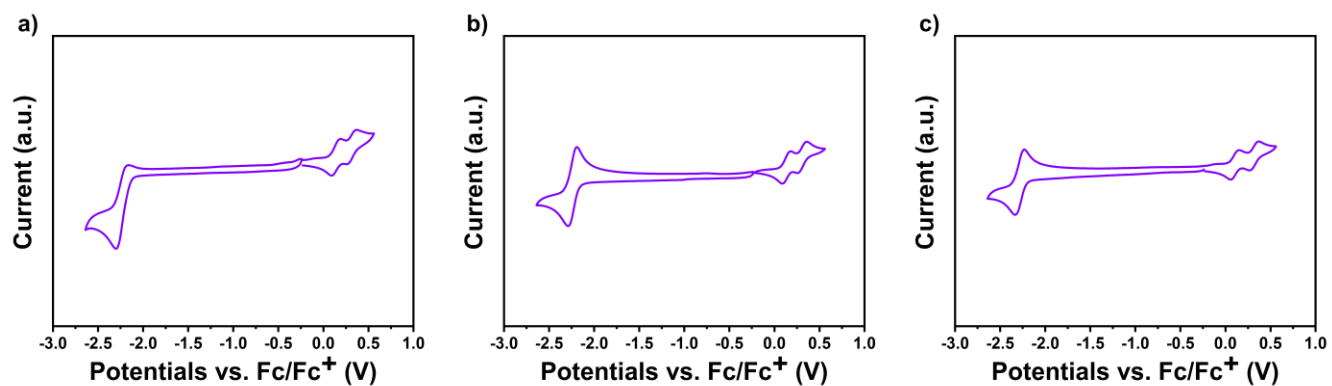


Figure S23. CV curves of a) Spiro-3TCzBN, b) DPh-3TCzBN and c) DMe-3TCzBN.

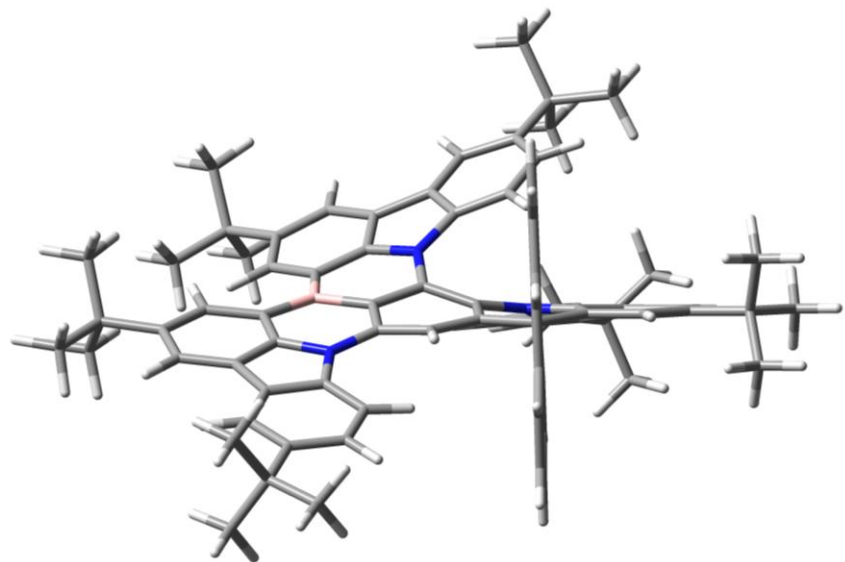


Figure S24. Optimized ground state (S_0) structures of Spiro-3TCzBN.

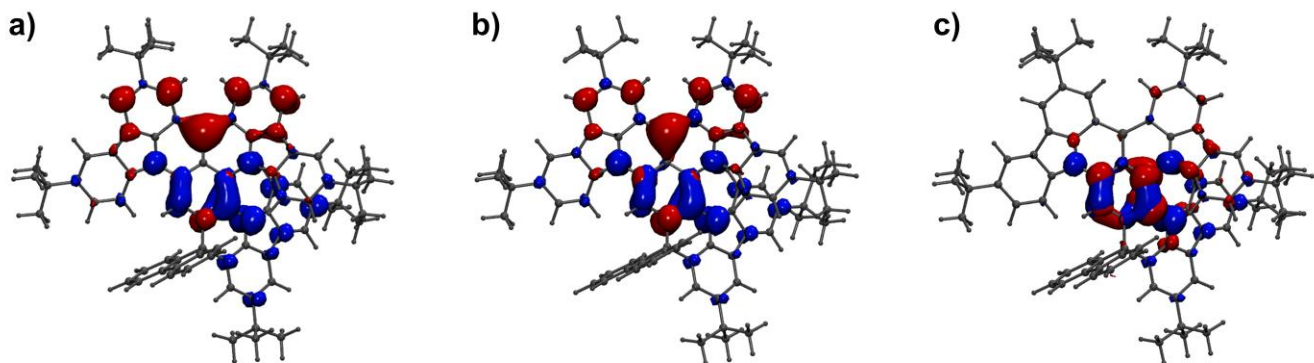


Figure S25. Natural transition orbitals (NTOs) of the excited a) S_1 , b) T_1 and c) T_2 states for Spiro-3TCzBN. The red and blue represent particles and holes, respectively.

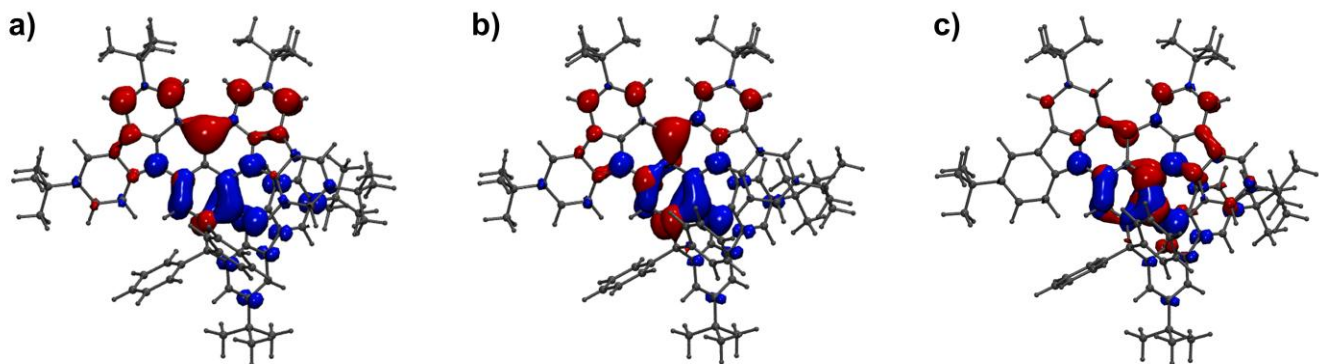


Figure S26. NTOs of the excited a) S_1 , b) T_1 and c) T_2 states for DPh-3TCzBN. The red and blue represent particles and holes, respectively.

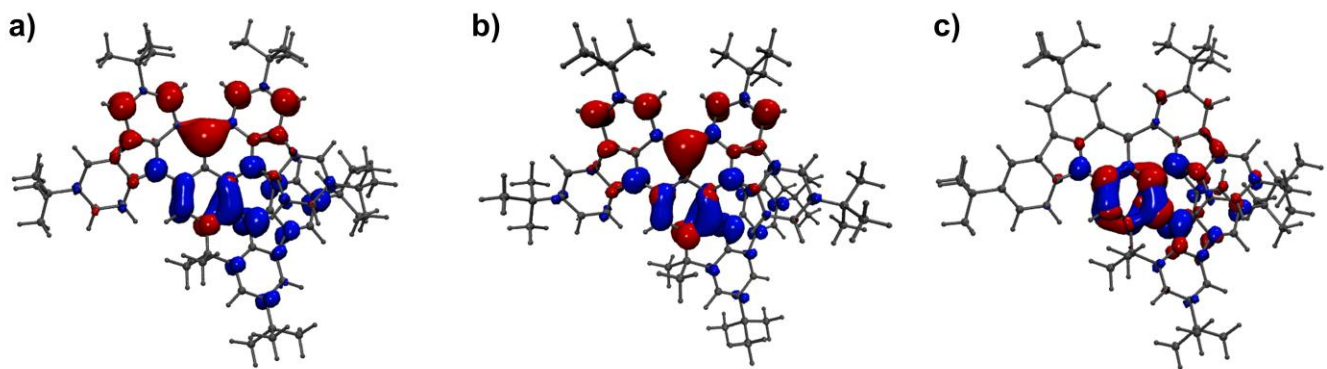


Figure S27. NTOs of the excited a) S_1 , b) T_1 and c) T_2 states for DMe-3TCzBN. The red and blue represent particles and holes, respectively.

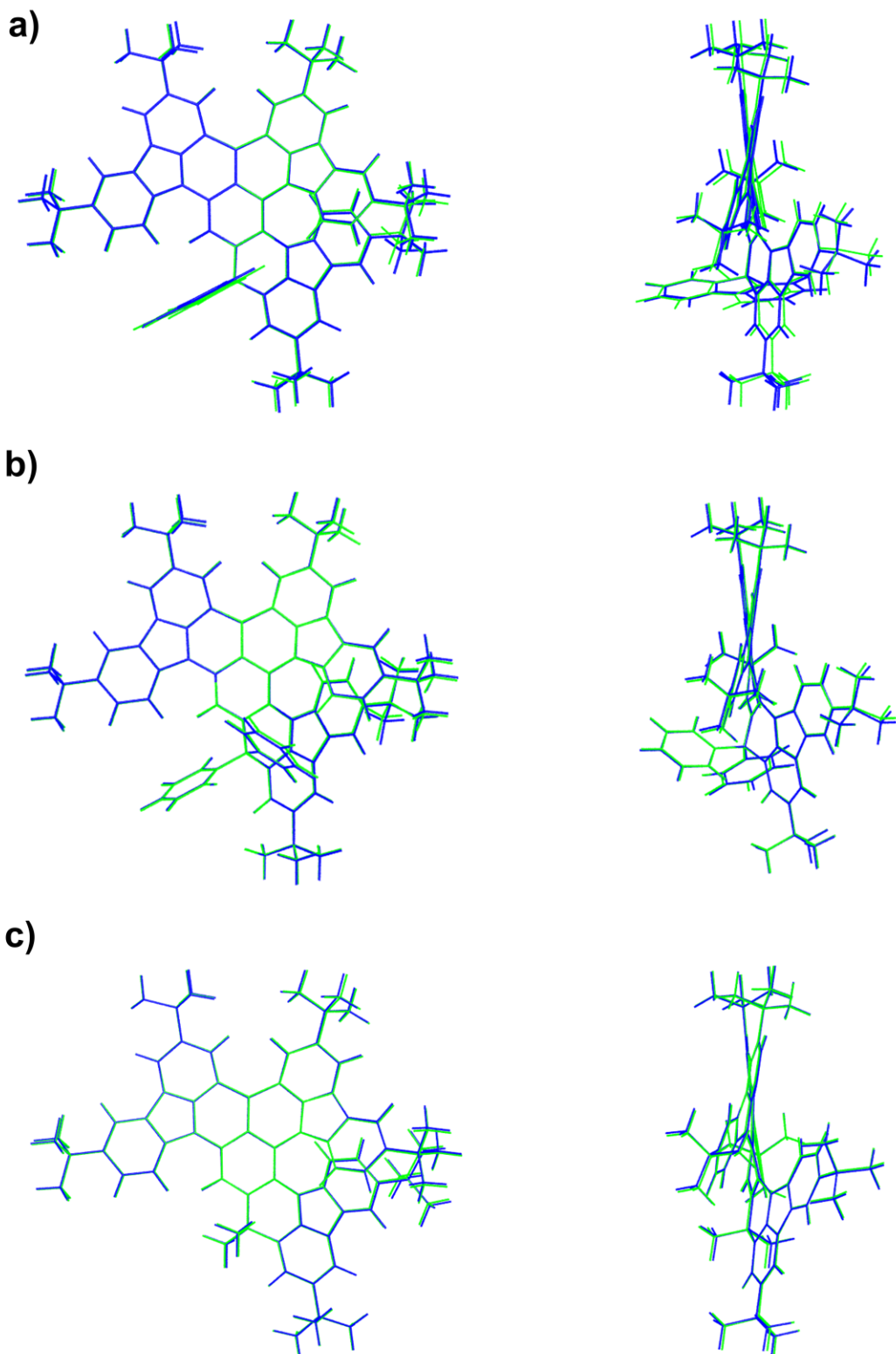


Figure S28. Overlap diagram of optimized S_0 (green) and S_1 (blue) geometries of a) Spiro-3TCzBN, b) DPh-3TCzBN and c) DMe-3TCzBN.

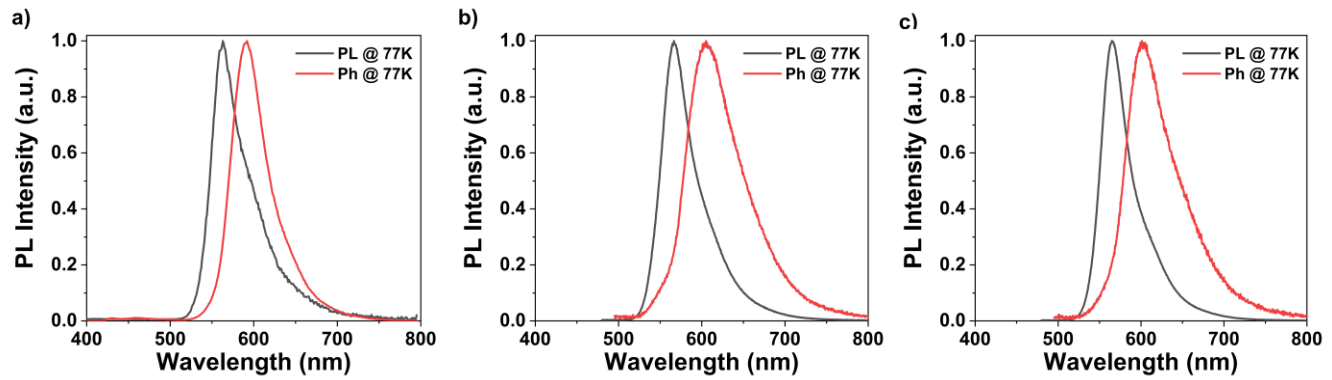


Figure S29. Fluorescence and phosphorescence spectra of a) Spiro-3TCzBN, b) DPh-3TCzBN and c) DMe-3TCzBN.

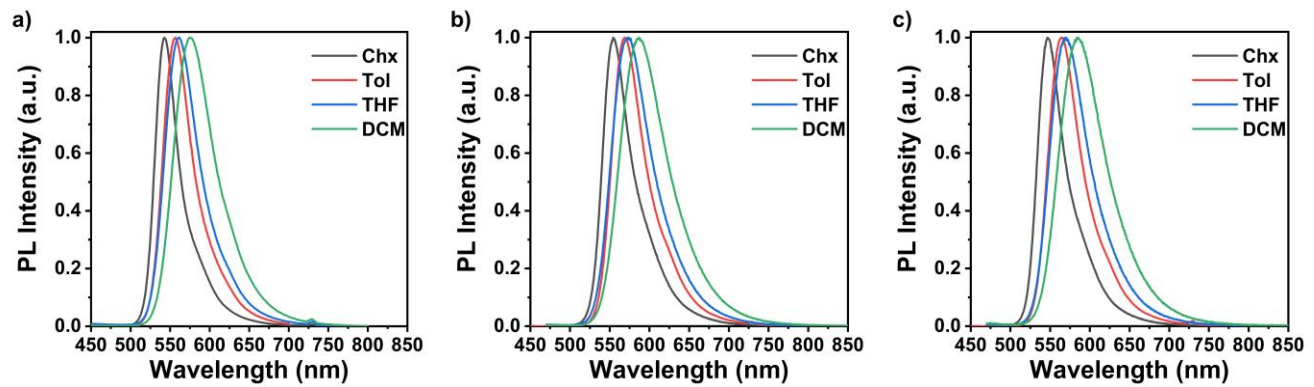


Figure S30. PL spectra of a) Spiro-3TCzBN, b) DPh-3TCzBN and c) DMe-3TCzBN in cyclohexane (Chx), toluene (Tol), tetrahydrofuran (THF) and dichloromethane (DCM) solutions (10^{-5} M) at room temperature.

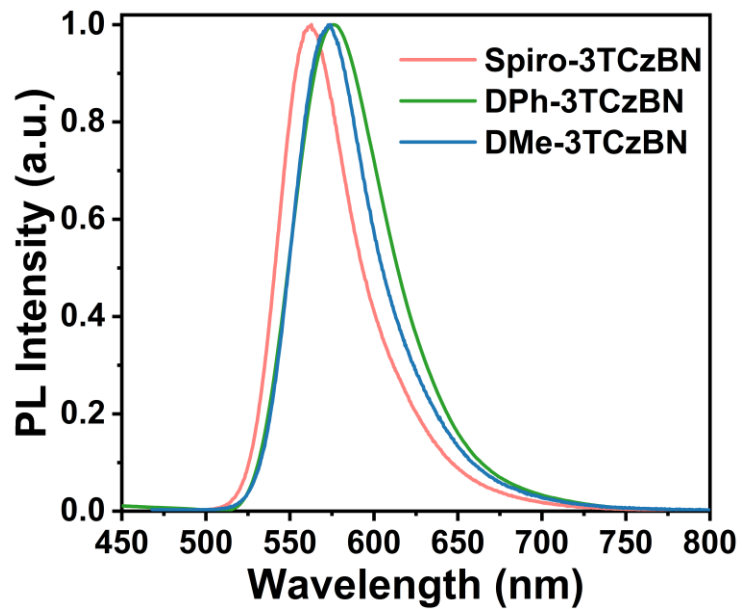


Figure S31. PL spectra of 3 wt% Spiro-3TCzBN, DPh-3TCzBN and DMe-3TCzBN: PhCzBCz doped films.

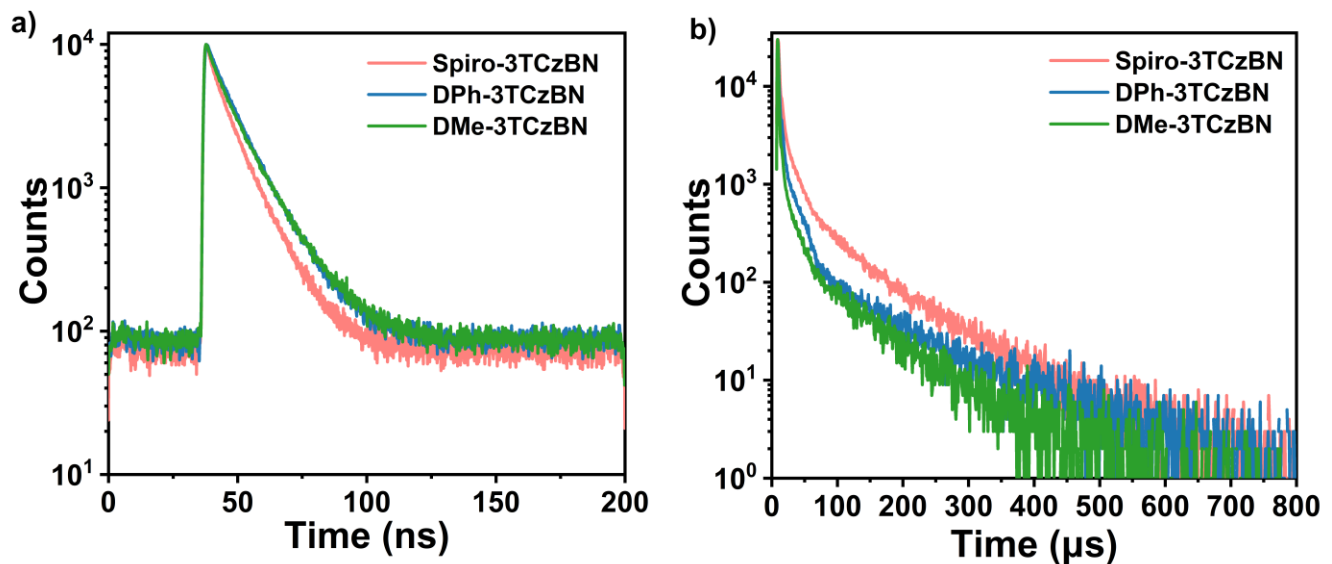


Figure S32. Transient PL decay spectra of 3 wt% Spiro-3TCzBN, DPh-3TCzBN and DMe-3TCzBN: PhCzBCz doped films.

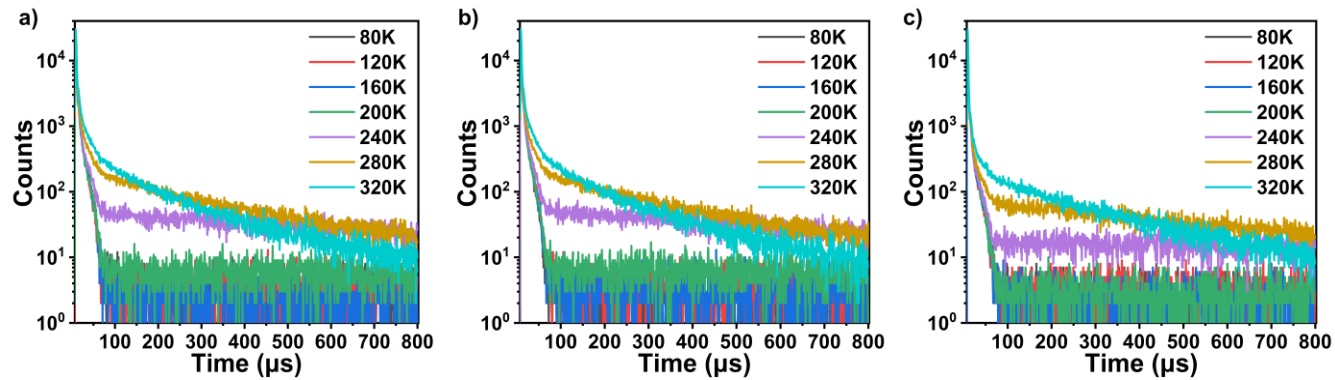


Figure S33. Transition PL decay curves of 3 wt% a) Spiro-3TCzBN, b) DPh-3TCzBN and c) DMe-3TCzBN: PhCzBCz doped films under different temperatures from 80 to 320 K.

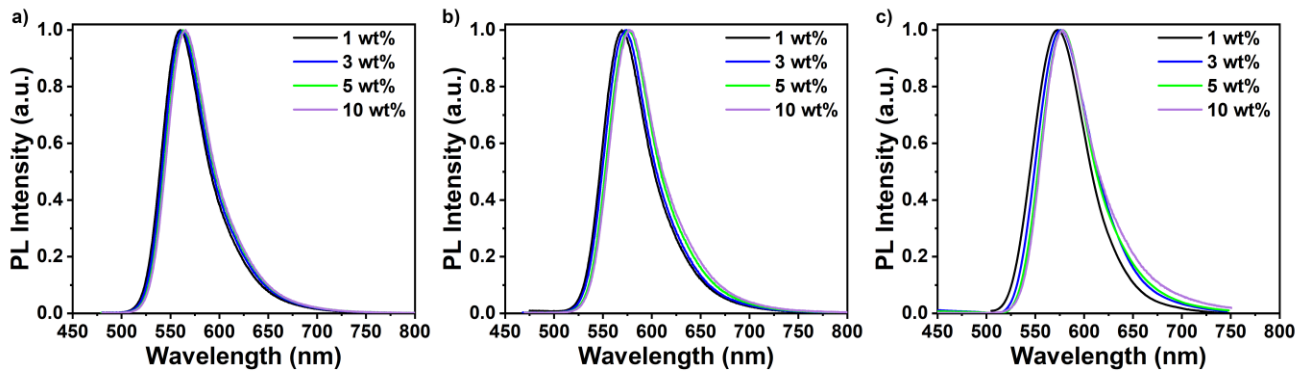


Figure S34. PL spectra of 1-10 wt% a) Spiro-3TCzBN, b) DPh-3TCzBN and c) DMe-3TCzBN: PhCzBCz doped films.

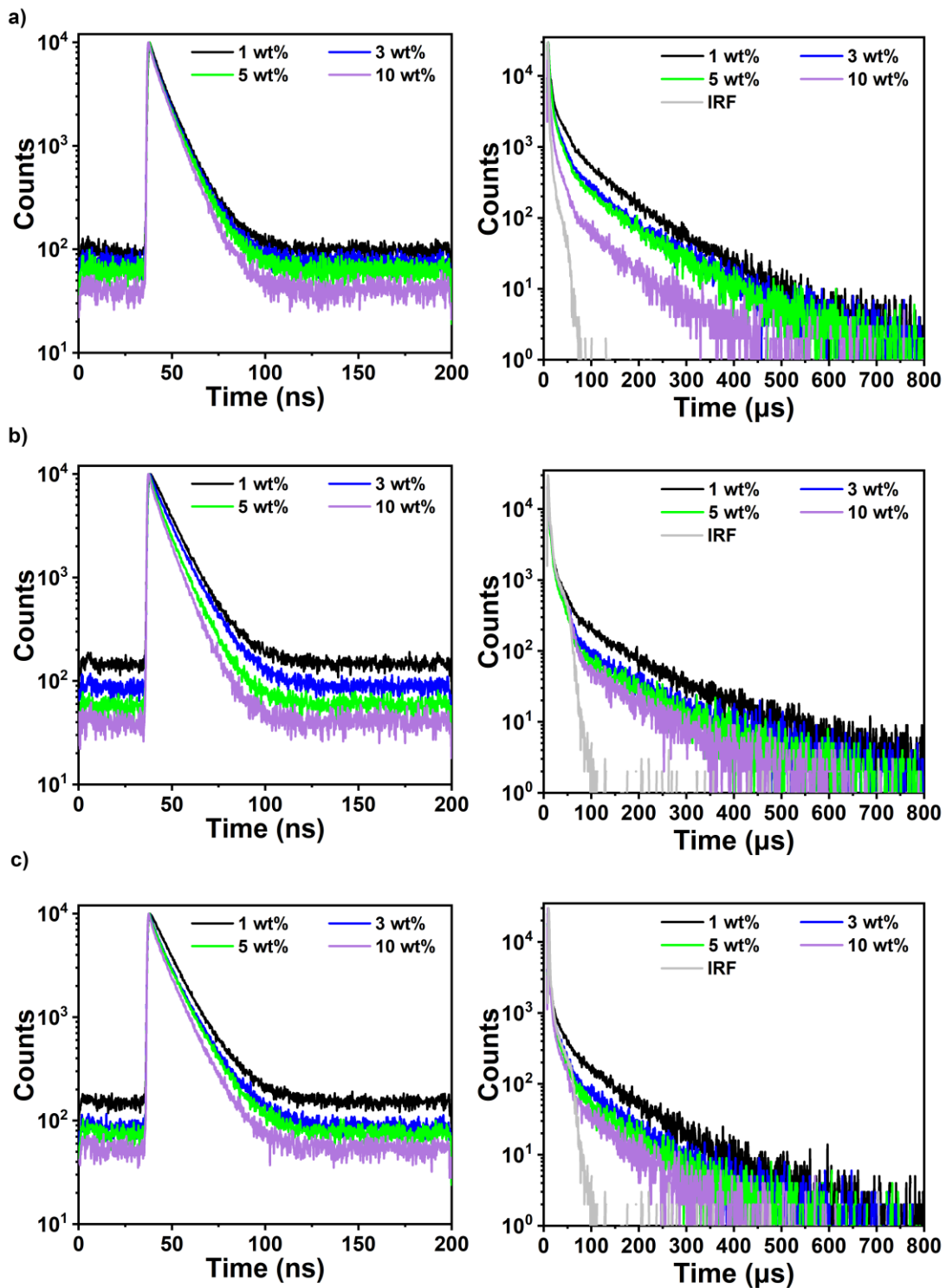


Figure S35. Transient PL decay spectra of 1-10 wt% a) Spiro-3TCzBN, b) DPh-3TCzBN and c) DMe-3TCzBN: PhCzBCz doped films

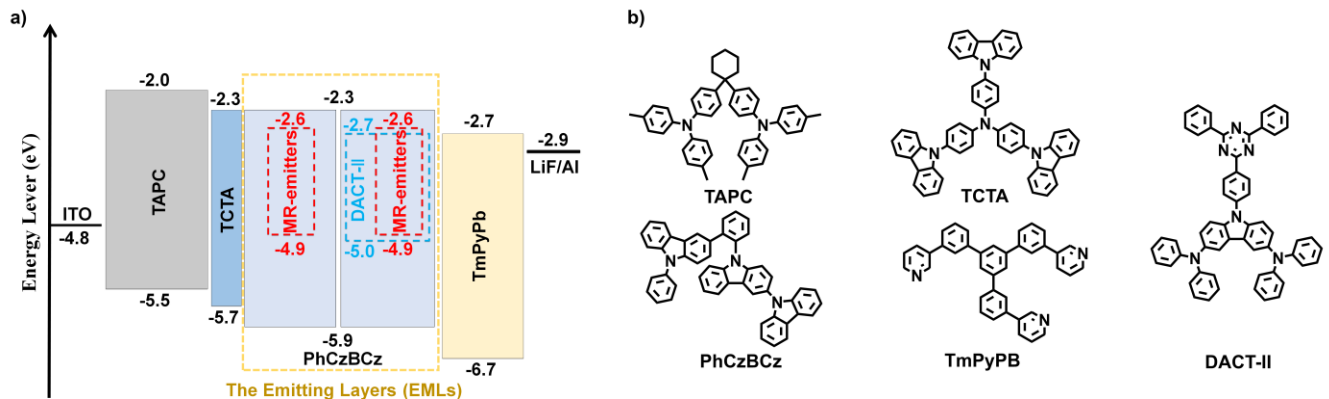


Figure S36. Energy level diagram of the OLEDs and molecular structures of the used materials.

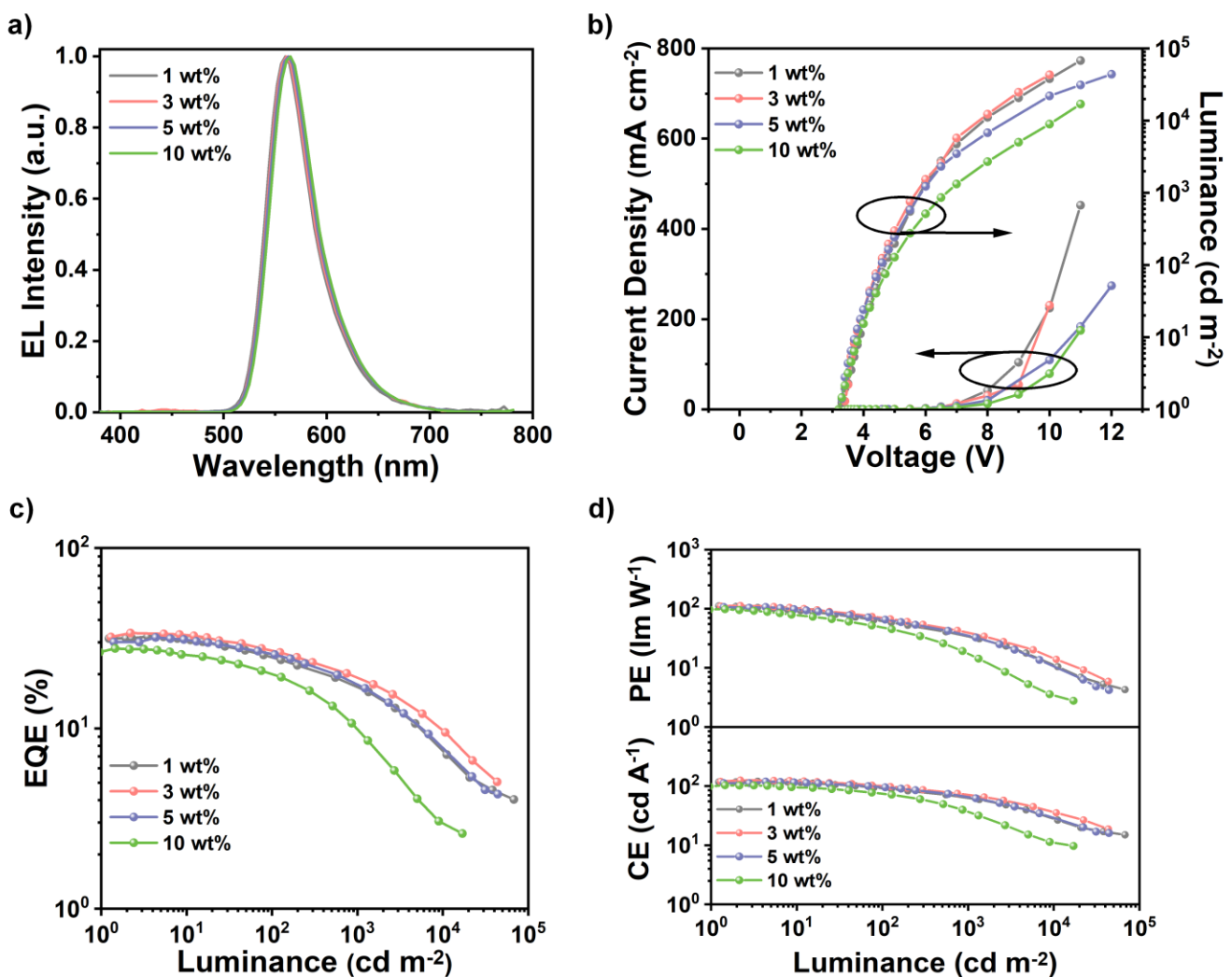


Figure S37. EL characteristics of Spiro-3TCzBN. a) EL spectra. b) J - V - L curves. c) EQE- L curves. d) CE- L and PE- L curves.

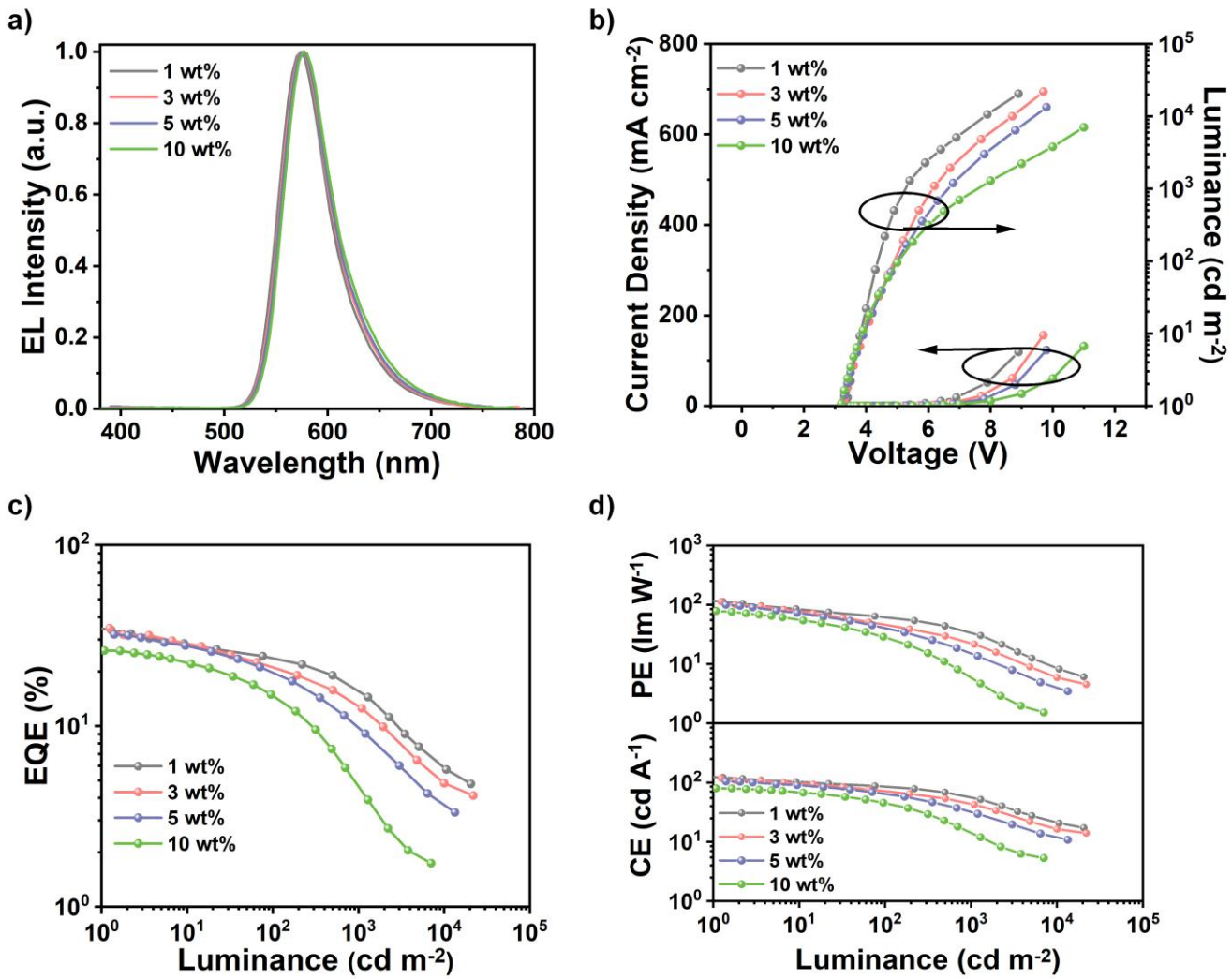


Figure S38. EL characteristics of DPh-3TCzBN. a) EL spectra. b) J - V - L curves. c) EQE- L curves. d) CE- L and PE- L curves.

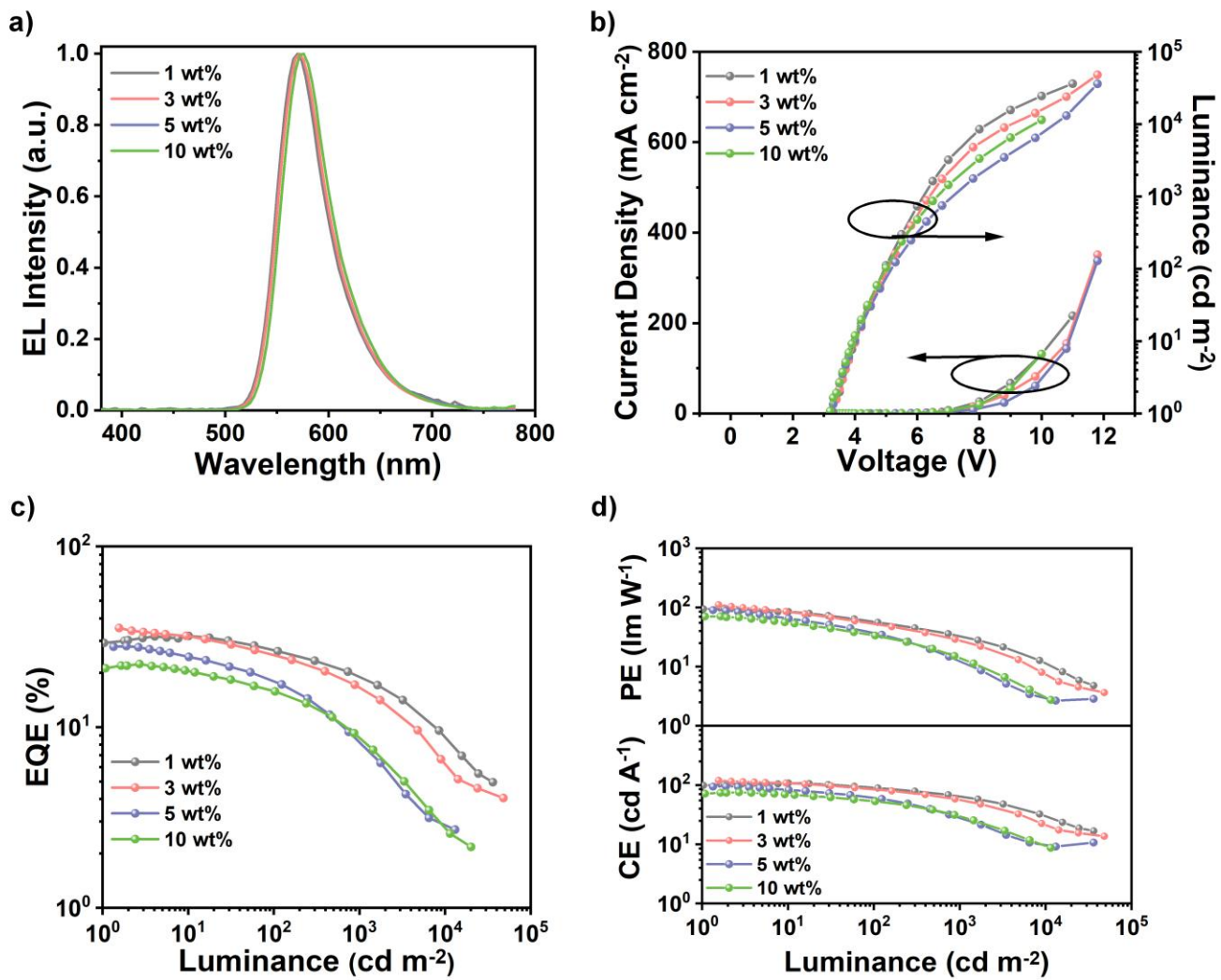


Figure S39. EL characteristics of DMe-3TCzBN. a) EL spectra. b) J - V - L curves. c) EQE- L curves. d) CE- L and PE- L curves.

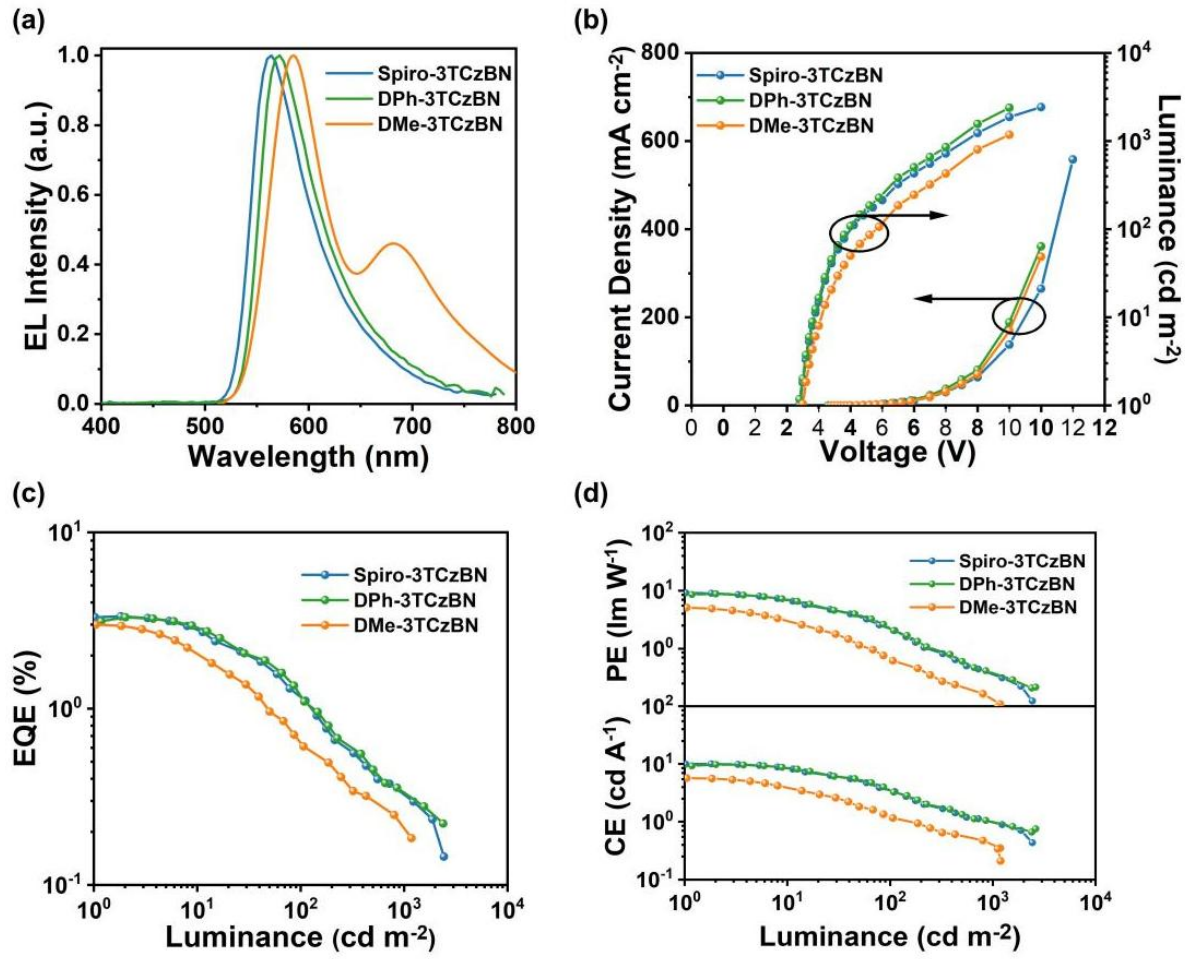


Figure S40. EL characteristics of non-doped OLEDs. a) EL spectra. b) J - V - L curves. c) EQE- L curves. d) CE- L and PE- L curves.

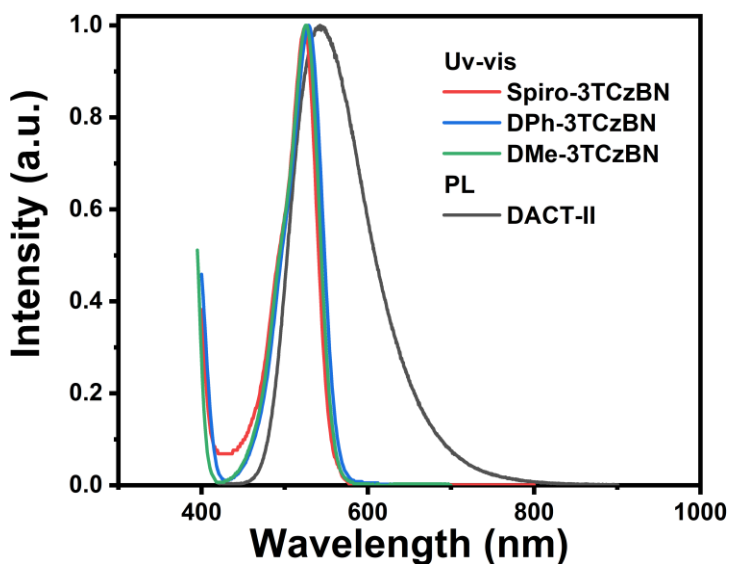


Figure S41. UV–vis absorption spectra of Spiro-3TCzBN, DPh-3TCzBN and DMe-3TCzBN in toluene at a concentration of 10^{-5} M and PL spectrum of 25 wt% DACT-II:PhCzBCz doped film.

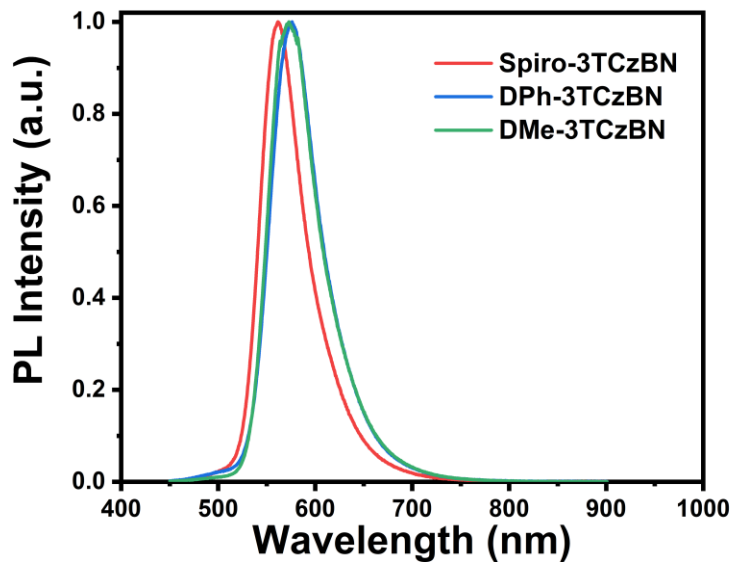


Figure S42. PL spectra of 3 wt% Spiro-3TCzBN, DPh-3TCzBN and DMe-3TCzBN:25 wt% DACT-II:PhCzBCz doped films.

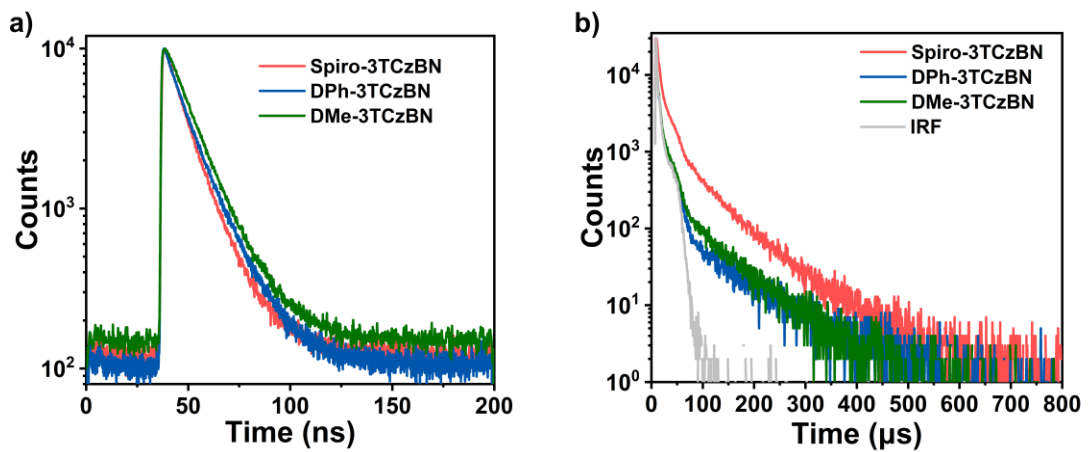


Figure S43. Transient PL decay spectra of 3 wt% Spiro-3TCzBN, DPh-3TCzBN and DMe-3TCzBN:25 wt% DACT-II:PhCzBCz doped films.

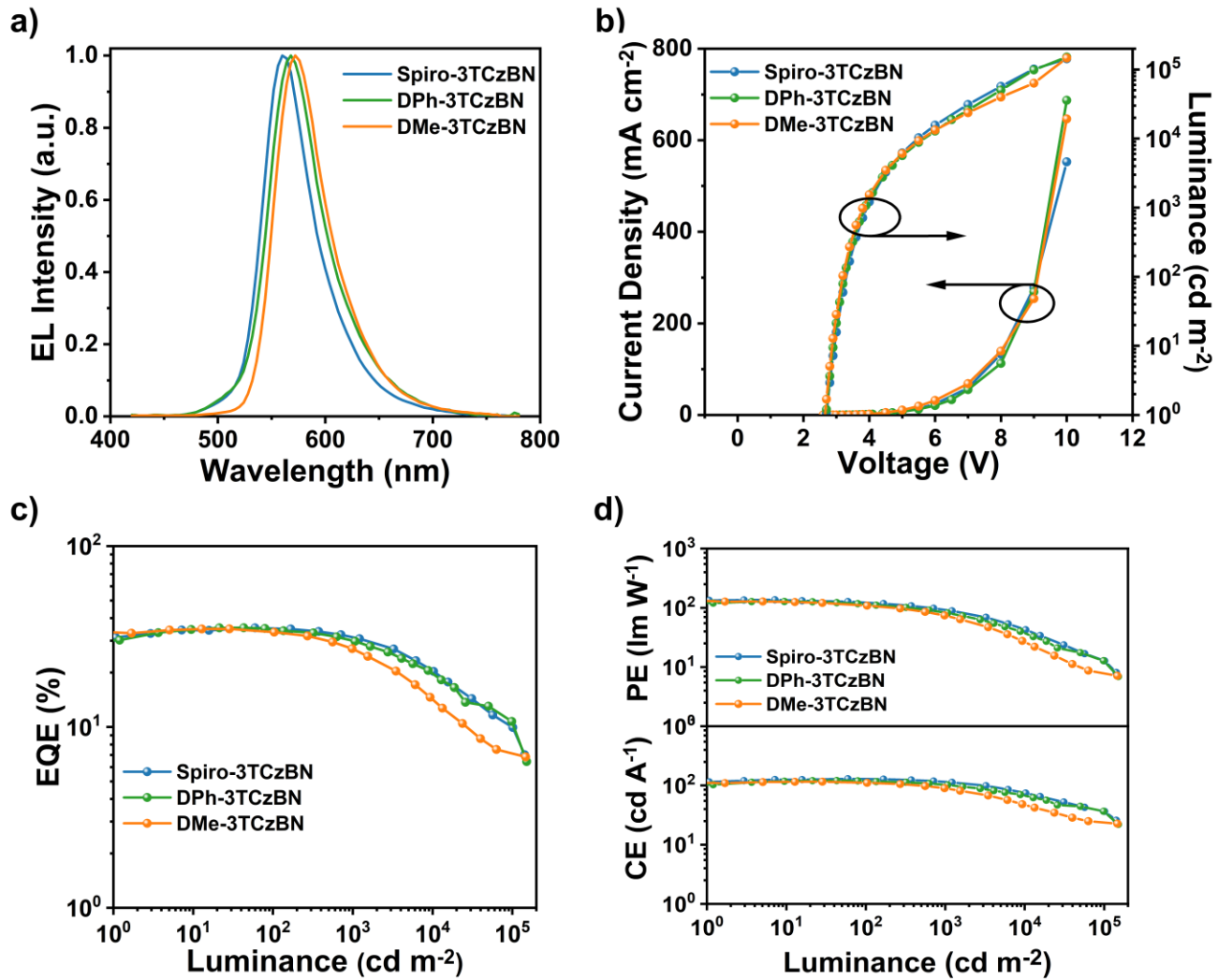


Figure S44. EL characteristics of Spiro-3TCzBN, DPh-3TCzBN and DMe-3TCzBN based devices with sensitizer. a) EL spectra. b) J - V - L curves. c) EQE- L curves. d) CE- L and PE- L curves.

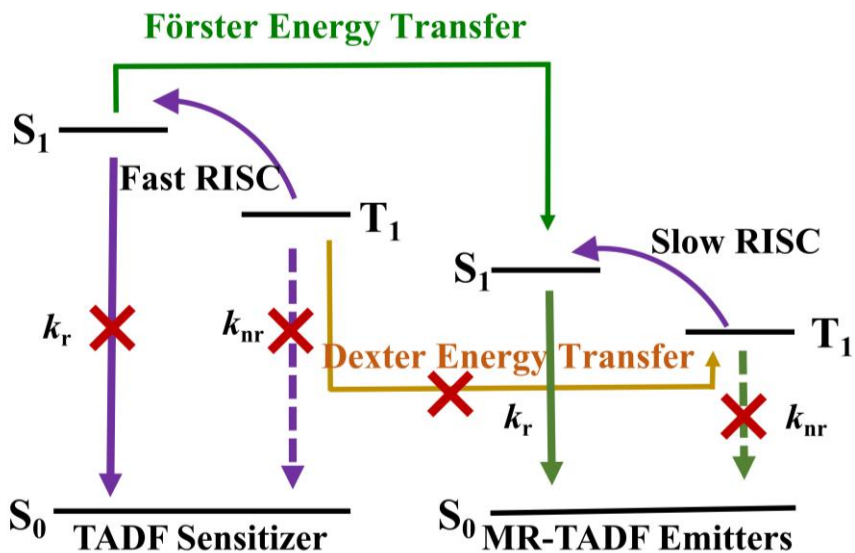


Figure S45. Schematic of the energy transfer mechanism for the TSF system.

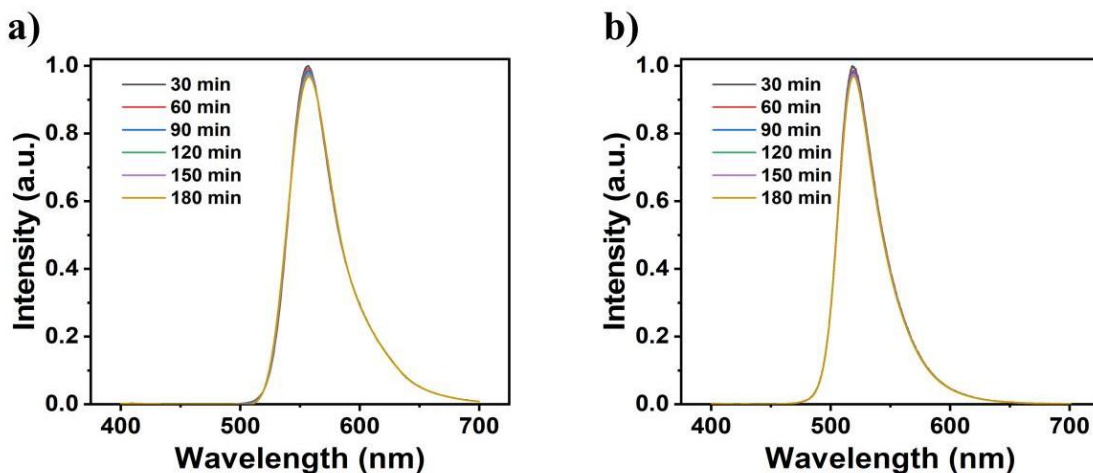


Figure S46. Optical stability of a) Spiro-3TCzBN and b) m-Cz-BNCz in toluene solution (1×10^{-5} M, 298 K) using 365 nm UV lamp for 3 hours of continuous irradiation.

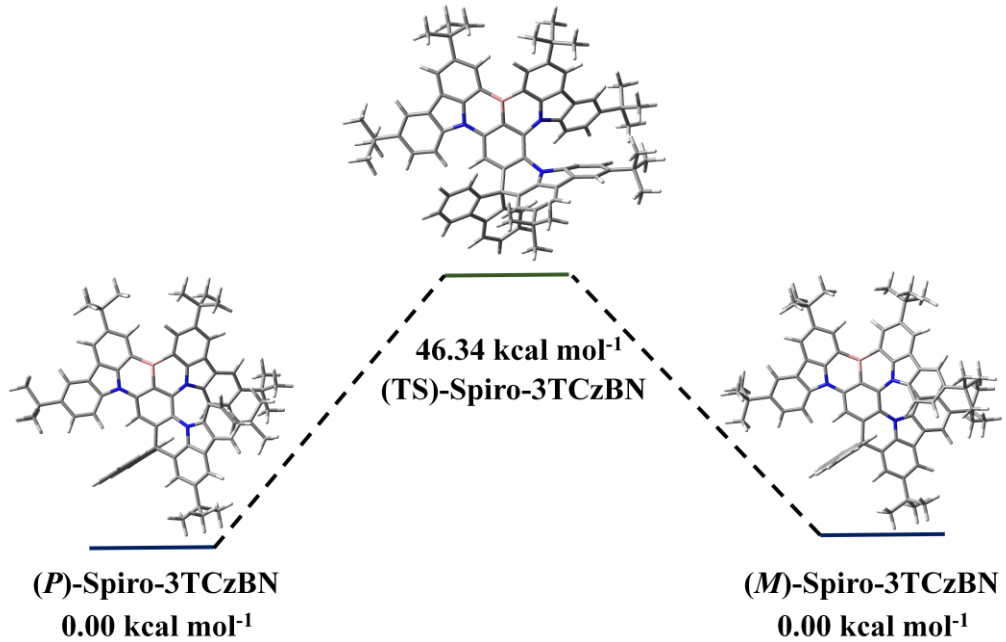


Figure S47. Energy barrier of racemization of the enantiomer Spiro-3TCzBN.

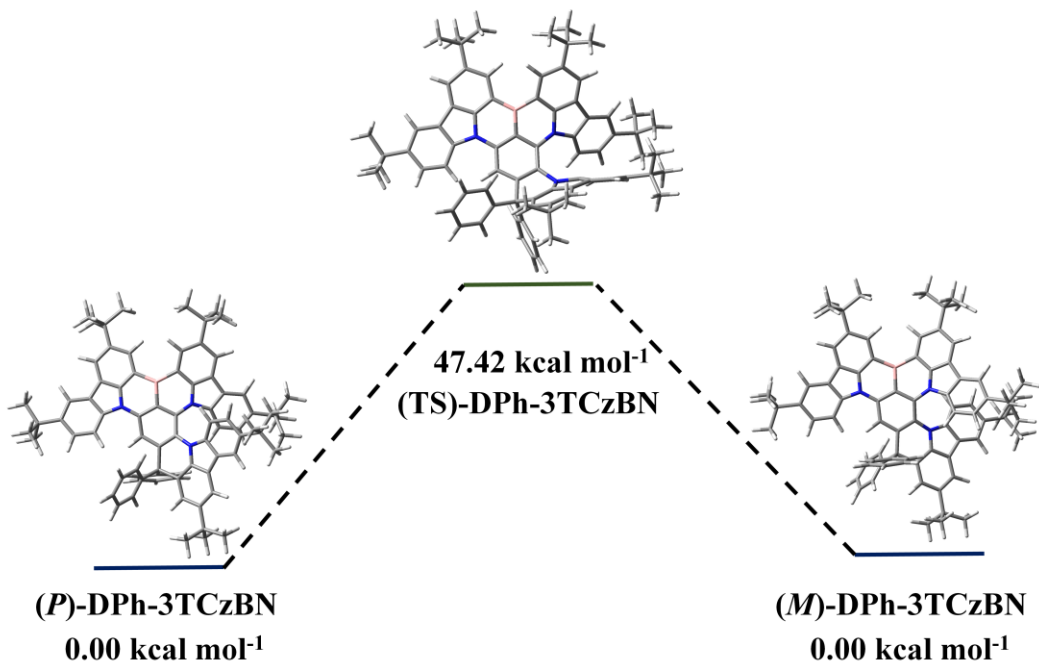


Figure S48. Energy barrier of racemization of the enantiomer DPh-3TCzBN.

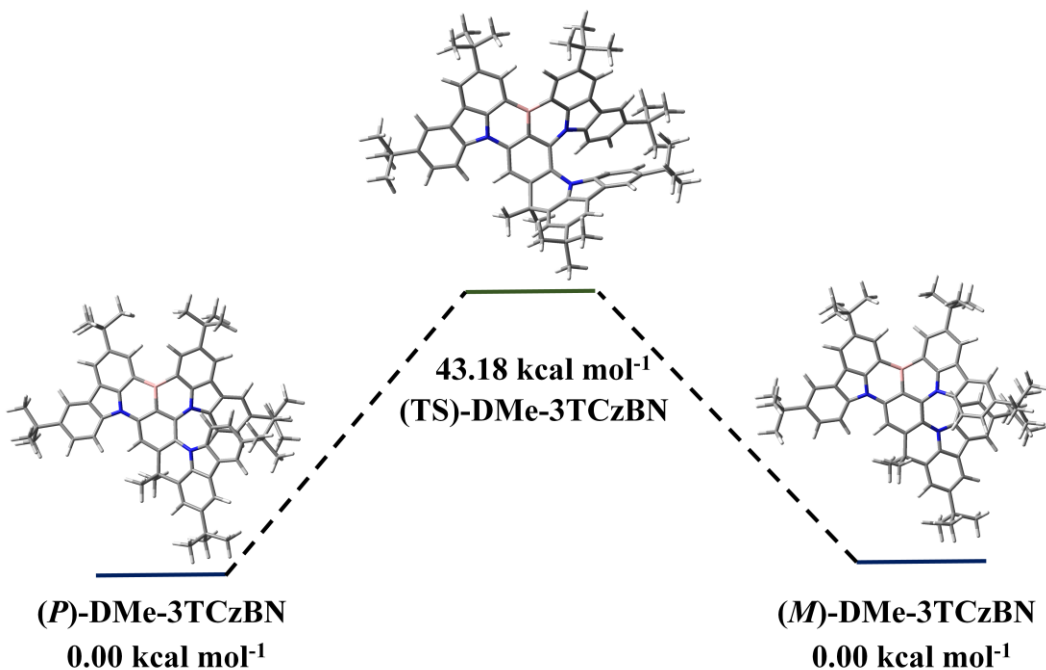


Figure S49. Energy barrier of racemization of the enantiomer DMe-3TCzBN.

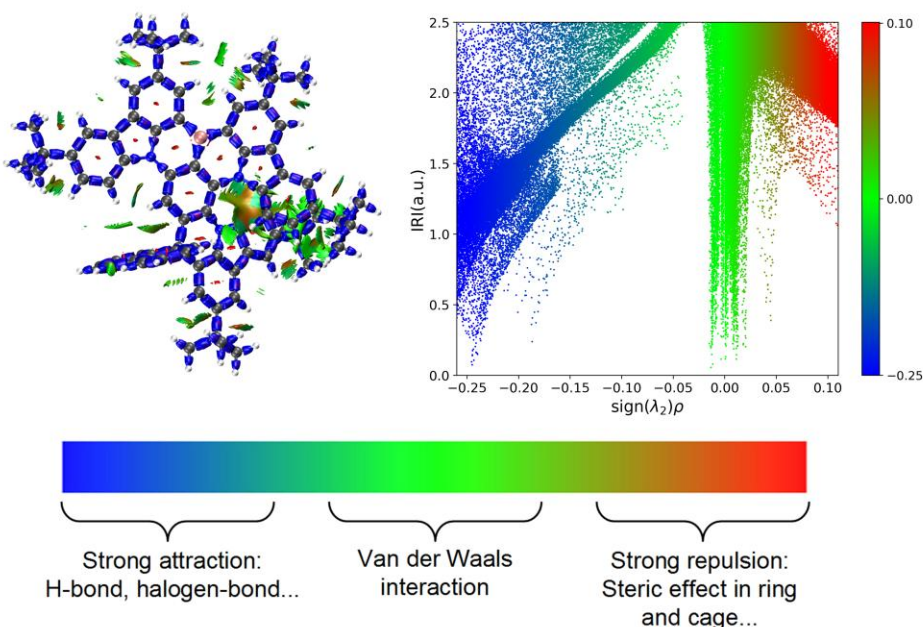


Figure S50. Calculated reduced density gradient isosurfaces based on optimized S_0 geometry of Spiro-3TCzBN, scattering diagram and standard coloring method and chemical explanation of $\text{sign}(\lambda_2)\rho$ on RDG isosurfaces.

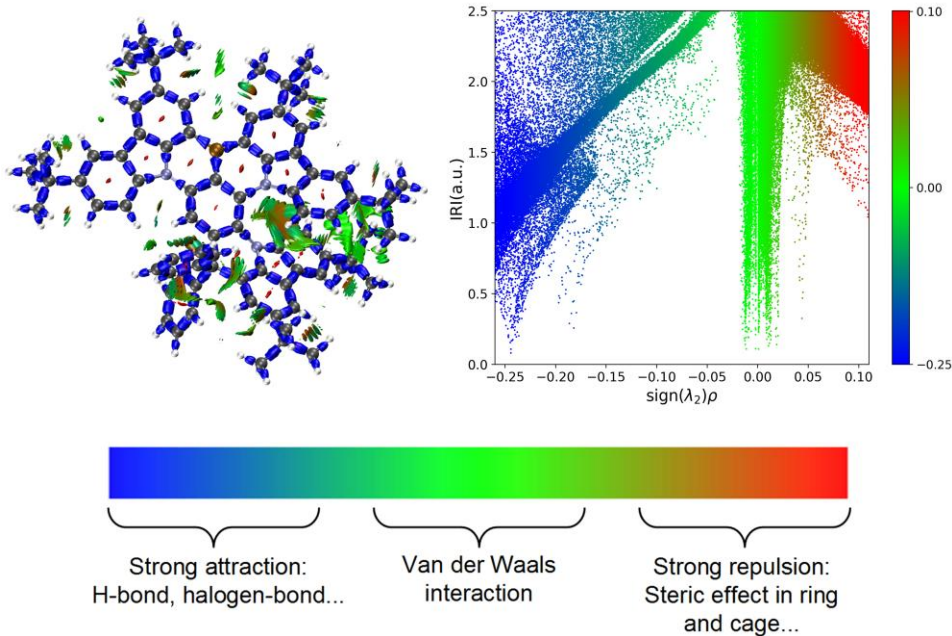


Figure S51. Calculated reduced density gradient isosurfaces based on optimized S_0 geometry of DPh-3TCzBN, scattering diagram and standard coloring method and chemical explanation of $\text{sign}(\lambda_2)\rho$ on RDG isosurfaces.

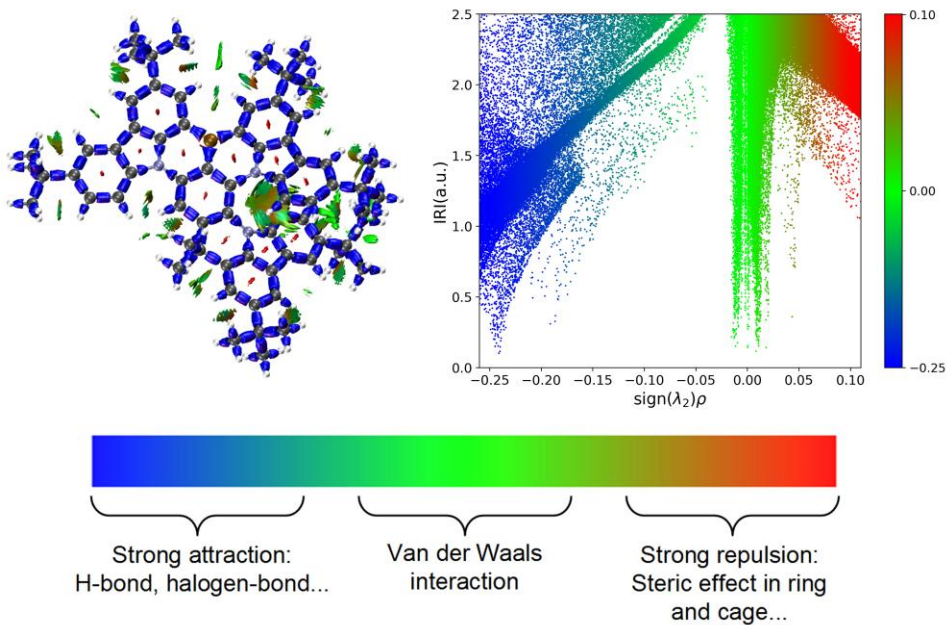


Figure S52. Calculated reduced density gradient isosurfaces based on optimized S_0 geometry of DMe-3TCzBN, scattering diagram and standard coloring method and chemical explanation of $\text{sign}(\lambda_2)\rho$ on RDG isosurfaces

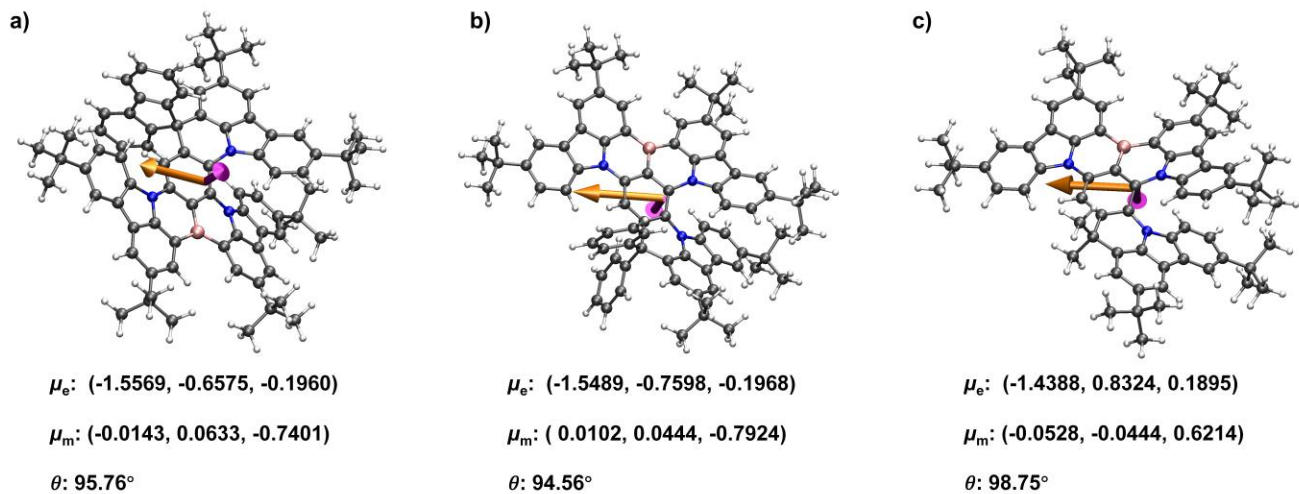


Figure S53. Directions of transition electric dipole moment (μ_e , orange arrow) and magnetic dipole moment (μ_m , purple arrow) for the $S_1 \rightarrow S_0$ transition of a) Spiro-3TCzBN, b) DPh-3TCzBN and c) DMe-3TCzBN calculated by TD-DFT.

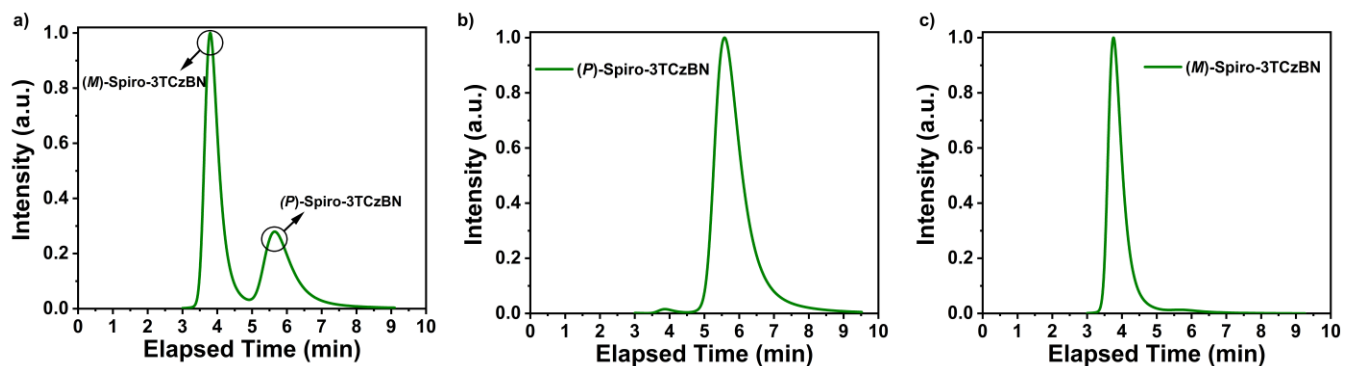


Figure S54. Chiral HPLC analysis of a) racemic Spiro-3TCzBN and the enantiomer b) (P) -Spiro-3TCzBN and c) (M) -Spiro-3TCzBN. (Mobile phase: propan-2-ol, Flow rate: 0.5 ml min⁻¹)

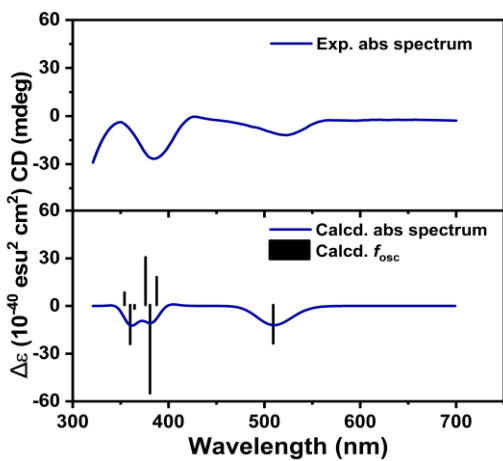


Figure S55. Experimental and calculated CD spectra of (*P*)-Spiro-3TCzBN.

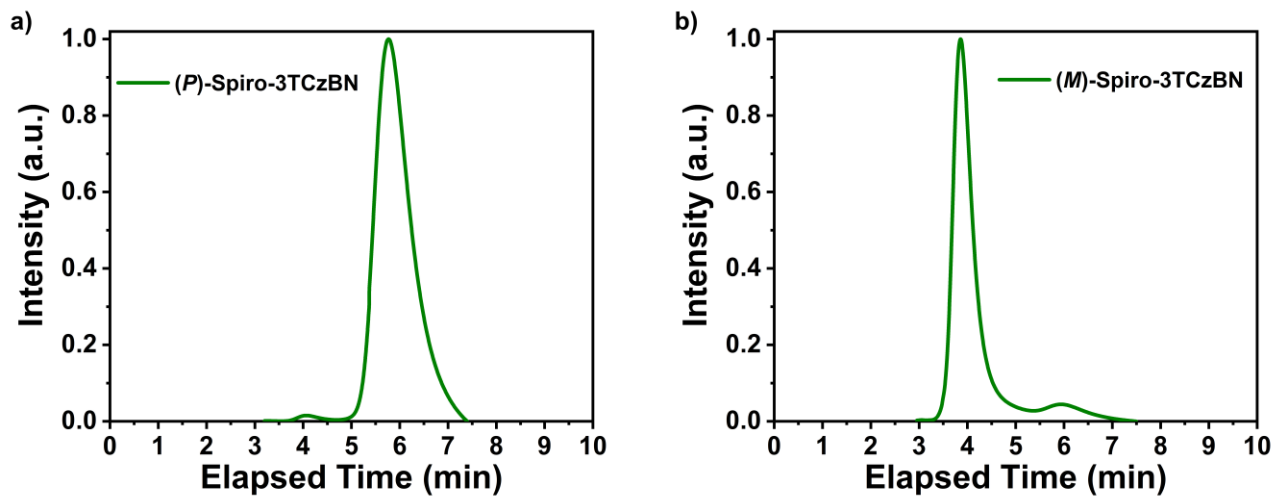


Figure S56. Chiral HPLC analysis of the residue samples: a) (*P*)-Spiro-3TCzBN and b) (*M*)- Spiro-3TCzBN obtained after thermal evaporation of the enantiomer under vacuum. (Mobile phase: propan-2-ol, Flow rate: 0.5 ml min⁻¹)

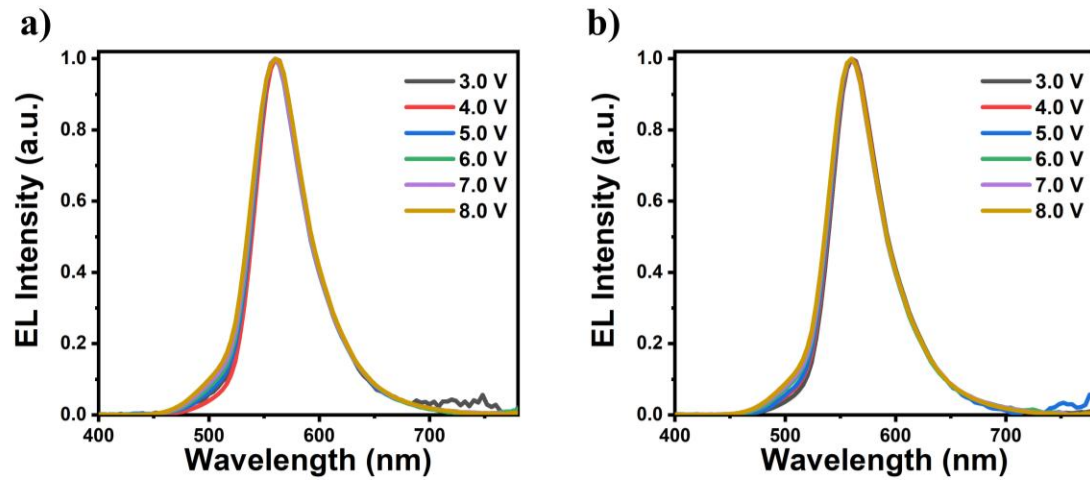


Figure S57. Normalized EL spectra operated at different voltages of a)(M)-Spiro-3TCzBN-based device and b)(P)-Spiro-3TCzBN-based device.

7. Supplementary Tables

Table S1. Summary of calculation for Spiro-3TCzBN, DPh-3TCzBN and DMe-3TCzBN based on the optimized S_0 , S_1 and T_1 structures at the B3LYP/6-311G(d, p) level.

Compound	Optimized structure	transition	Wavelength [nm]	Energy [eV]	Oscillator strength	Coefficient of HOMO-LUMO	ΔE_{ST} [eV]
Spiro-3TCzBN	S_0	S_0-S_1	510.16	2.4303	0.1792	98.96%	0.2840
	S_0	S_0-T_1	585.24	2.1185	0.0000	95.02%	
	S_1	S_1-S_0	565.87	2.1911	0.1340	99.14%	
	T_1	T_1-S_0	650.13	1.9071	0.0000	94.78%	
DPh-3TCzBN	S_0	S_0-S_1	516.40	2.4009	0.1841	98.96%	0.4133
	S_0	S_0-T_1	597.95	2.0735	0.0000	94.28%	
	S_1	S_1-S_0	579.21	2.1406	0.1359	99.17%	
	T_1	T_1-S_0	717.79	1.7273	0.0000	87.17%	
DMe-3TCzBN	S_0	S_0-S_1	512.52	2.4191	0.1686	99.00%	0.2788
	S_0	S_0-T_1	585.97	2.1159	0.0000	94.68%	
	S_1	S_1-S_0	567.85	2.1834	0.1268	99.18%	
	T_1	T_1-S_0	650.96	1.9046	0.0000	94.92%	

Table S2. Summary of PL spectra data of Spiro-3TCzBN, DPh-3TCzBN and DMe-3TCzBN in different polar solvents.

compound	Spiro-3TCzBN		DPh-3TCzBN		DMe-3TCzBN	
solvent	$\lambda_{\text{em}}^{\text{a})}$ [nm]	FWHM ^{b)} [nm/eV]	$\lambda_{\text{em}}^{\text{a})}$ [nm]	FWHM ^{b)} [nm/eV]	$\lambda_{\text{em}}^{\text{a})}$ [nm]	FWHM ^{b)} [nm/eV]
Chx	542	35/0.15	555	44/0.17	547	41/0.17
Tol	556	44/0.17	568	54/0.19	565	49/0.19
THF	561	51/0.20	573	60/0.22	569	59/0.22
DCM	546	61/0.22	587	69/0.23	585	69/0.23

^{a)} PL peak wavelength. ^{b)} Full width at half maximum.

Table S3. Summary of photophysical data of x wt % Spiro-3TCzBN: PhCzBCz doped films without sensitizer, and 3 wt % Spiro-3TCzBN: 25 wt% DACT-II: cohost doped film with sensitizer.

Film	x wt %	$\lambda_{\text{em}}^{\text{a})}$ [nm]	FWHM ^{b)} [nm/eV]	$\Phi_{\text{PL}}^{\text{c})}$ [%]	$\Phi_{\text{F}}^{\text{d})}$ [%]	$\Phi_{\text{TADF}}^{\text{e})}$ [%]	$\tau_{\text{F}}^{\text{f})}$ [ns]	$\tau_{\text{TADF}}^{\text{g})}$ [μs]	$k_{\text{r}}^{\text{h})}$ [10^7s^{-1}]	$k_{\text{nr}}^{\text{i})}$ [10^6s^{-1}]	$k_{\text{ISC}}^{\text{j})}$ [10^7s^{-1}]	$k_{\text{RISC}}^{\text{k})}$ [10^4s^{-1}]
	1	560	50/0.18	96	59.1	36.8	9.4	92.9	6.3	2.6	4.1	1.7
Without sensitizer	3	562	52/0.19	96	69.1	26.9	9.3	95.9	7.5	3.1	3.0	1.4
	5	564	52/0.19	93	68.7	24.3	9.1	97.5	7.6	5.7	2.9	1.4
	10	565	53/0.19	88	74.3	13.6	8.6	107.2	8.7	11.8	1.8	1.1
Sensitizer	3	561	53/0.19	97	36.6	60.4	10.8	31.46	3.4	1.0	5.7	8.4

^{a)} PL emission maximum. ^{b)} Full width at half maximum of the PL spectrum. ^{c)} The total photoluminescence quantum yield (Φ_{PL}). ^{d)} The prompt fluorescent (Φ_{F}) component of Φ_{PL} . ^{e)} The delayed fluorescent (Φ_{TADF}) component of Φ_{PL} . ^{f)} The lifetime of prompt fluorescence (τ_{F}). ^{g)} The lifetime of delayed fluorescence (τ_{TADF}). ^{h)} The rate constant of radiative decay (k_{r}). ⁱ⁾ The rate constant of non-radiative decay (k_{nr}). ^{j)} The rate constant of intersystem crossing (k_{ISC}). ^{k)} The rate constant of reverse intersystem crossing (k_{RISC}).

Table S4. Summary of photophysical data of x wt % DPh-3TCzBN: PhCzBCz doped films without sensitizer, and 3 wt % DPh-3TCzBN: 25 wt% DACT-II: cohost doped film with sensitizer.

Film	x wt %	$\lambda_{\text{em}}^{\text{a})}$ [nm]	FWHM ^{b)} [nm/eV]	$\Phi_{\text{PL}}^{\text{c})}$ [%]	$\Phi_{\text{F}}^{\text{d})}$ [%]	$\Phi_{\text{TADF}}^{\text{e})}$ [%]	$\tau_{\text{F}}^{\text{f})}$ [ns]	$\tau_{\text{TADF}}^{\text{g})}$ [μs]	$k_{\text{r}}^{\text{h})}$ [10^7s^{-1}]	$k_{\text{nr}}^{\text{i})}$ [10^6s^{-1}]	$k_{\text{ISC}}^{\text{j})}$ [10^7s^{-1}]	$k_{\text{RISC}}^{\text{k})}$ [10^4s^{-1}]
Without sensitizer	1	572	59/0.21	96	60.8	35.2	11.3	93.5	5.4	2.2	3.2	1.7
	3	573	60/0.21	93	68.3	24.7	10.8	98.2	6.3	4.7	2.4	1.4
	5	575	61/0.21	90	67.7	22.3	9.4	104.8	7.2	8.1	2.6	1.3
	10	576	61/0.21	84	71.1	12.9	8.3	110.1	8.6	16.3	1.9	1.1
Sensitizer	3	576	59/0.21	97	64.6	32.4	12.5	42.8	5.2	1.6	2.7	3.5

^{a)} PL emission maximum. ^{b)} Full width at half maximum of the PL spectrum. ^{c)} The total photoluminescence quantum yield (Φ_{PL}). ^{d)} The prompt fluorescent (Φ_{F}) component of Φ_{PL} . ^{e)} The delayed fluorescent (Φ_{TADF}) component of Φ_{PL} . ^{f)} The lifetime of prompt fluorescence (τ_{F}). ^{g)} The lifetime of delayed fluorescence (τ_{TADF}). ^{h)} The rate constant of radiative decay (k_{r}). ⁱ⁾ The rate constant of non-radiative decay (k_{nr}). ^{j)} The rate constant of intersystem crossing (k_{ISC}). ^{k)} The rate constant of reverse intersystem crossing (k_{RISC}).

Table S5. Summary of photophysical data of x wt % DMe-3TCzBN: PhCzBCz doped films without sensitizer, and 3 wt % DMe-3TCzBN: 25 wt% DACT-II: cohost doped film with sensitizer.

Film	x wt %	$\lambda_{\text{em}}^{\text{a})}$ [nm]	FWHM ^{b)} [nm/eV]	$\Phi_{\text{PL}}^{\text{c})}$ [%]	$\Phi_{\text{F}}^{\text{d})}$ [%]	$\Phi_{\text{TADF}}^{\text{e})}$ [%]	$\tau_{\text{F}}^{\text{f})}$ [ns]	$\tau_{\text{TADF}}^{\text{g})}$ [μs]	$k_{\text{r}}^{\text{h})}$ [10^7s^{-1}]	$k_{\text{nr}}^{\text{i})}$ [10^6s^{-1}]	$k_{\text{ISC}}^{\text{j})}$ [10^7s^{-1}]	$k_{\text{RISC}}^{\text{k})}$ [10^4s^{-1}]
Without sensitizer	1	569	54/0.20	95	62.2	32.8	11.8	88.6	5.3	2.7	2.9	1.7
	3	572	56/0.21	90	71.3	18.7	11.2	98.2	6.4	7.1	1.9	1.3
	5	574	56/0.21	84	68.6	15.4	10.1	103.9	6.8	12.9	1.8	1.2
	10	575	58/0.21	72	60.2	11.8	9.9	113.2	6.1	23.6	1.6	1.1
Sensitizer	3	572	59/0.21	96	60.5	35.5	13.0	54.4	4.6	1.9	2.8	2.9

^{a)} PL emission maximum. ^{b)} Full width at half maximum of the PL spectrum. ^{c)} The total photoluminescence quantum yield (Φ_{PL}). ^{d)} The prompt fluorescent (Φ_{F}) component of Φ_{PL} . ^{e)} The delayed fluorescent (Φ_{TADF}) component of Φ_{PL} . ^{f)} The lifetime of prompt fluorescence (τ_{F}). ^{g)} The lifetime of delayed fluorescence (τ_{TADF}). ^{h)} The rate constant of radiative decay (k_{r}). ⁱ⁾ The rate constant of non-radiative decay (k_{nr}). ^{j)} The rate constant of intersystem crossing (k_{ISC}). ^{k)} The rate constant of reverse intersystem crossing (k_{RISC}).

Table 6. Summary of the EL data of the Spiro-3TCzBN, DPh-3TCzBN and DMe-3TCzBN-based devices without sensitizer.

emitter	Doping ratios [wt %]	$\lambda_{\text{em}}^{\text{a})}$ [nm]	FWHM ^{b)} [nm/eV]	$V_{\text{on}}^{\text{c})}$ [V]	$L_{\text{max}}^{\text{d})}$ [cd m ⁻²]	$\text{CE}_{\text{max}}^{\text{e})}$ [cd A ⁻¹]	$\text{PE}_{\text{max}}^{\text{f})}$ [lm W ⁻¹]	$\text{EQE}^{\text{g})}$ [%]	CIE ^{h)} (x, y)
Spiro-3TCzBN	1	560	50/0.17	3.3	67980	120.3	111.3	32.3/24.8/17.1	(0.460, 0.532)
	3	560	50/0.17	3.3	43350	125.9	113.1	33.8/26.9/19.1	(0.461, 0.530)
	5	564	51/0.18	3.3	44055	118.9	106.8	31.9/25.7/17.5	(0.466, 0.527)
	10	564	52/0.18	3.2	17004	103.3	98.4	27.7/20.0/9.8	(0.469, 0.525)
DPh-3TCzBN	1	574	59/0.21	3.4	20532	126.8	120.7	33.9/23.6/15.4	(0.456, 0.536)
	3	574	59/0.21	3.3	21921	118.1	112.4	35.4/24.9/16.5	(0.467, 0.520)
	5	574	59/0.21	3.3	13371	104.5	99.5	32.0/19.5/9.7	(0.478, 0.511)
	10	578	60/0.22	3.2	7046	79.9	78.4	26.1/14.6/4.6	(0.504, 0.490)
DMe-3TCzBN	1	568	55/0.20	3.3	36249	107.6	94.2	31.7/26.4/18.9	(0.495, 0.502)
	3	568	56/0.21	3.4	48160	119.9	110.7	34.7/21.0/12.9	(0.496, 0.502)
	5	572	57/0.21	3.3	36240	95.1	89.9	28.1/17.9/8.2	(0.508, 0.498)
	10	572	59/0.22	3.2	13130	75.8	70.6	22.4/16.6/8.6	(0.510, 0.488)

^{a)} EL peak wavelength at 100 cd m⁻². ^{b)} Full width at half maximum of the spectra given in wavelength. ^{c)} Turn-on voltage at 1 cd m⁻². ^{d)} Maximum luminance. ^{e)} Maximum current efficiency. ^{f)} Maximum power efficiency. ^{g)} Maximum external quantum efficiency, and values at 100 and 1000 cd m⁻², respectively. ^{h)} Value taken at 100 cd m⁻².

Table S7. Summary of the EL data of the non-doped OLEDs.

emitter	$\lambda_{\text{em}}^{\text{a})}$ [nm]	FWHM ^{b)} [nm/eV]	$V_{\text{on}}^{\text{c})}$ [V]	$L_{\text{max}}^{\text{d})}$ [cd m ⁻²]	CE _{max} ^{e)} [cd A ⁻¹]	PE _{max} ^{f)} [lm W ⁻¹]	EQE ^{g)} [%]	CIE ^{h)} (x, y)
Spiro-3TCzBN	564	63/0.23	3.4	2428	10.1	9.2	3.3/1.2/0.3	(0.487, 0.508)
DPh-3TCzBN	572	65/0.24	3.4	2390	9.8	8.8	3.3/1.1/0.3	(0.492, 0.484)
DMe-3TCzBN	584	69/0.26	3.5	1181	5.7	5.1	3.0/0.7/0.2	(0.553, 0.441)

^{a)} EL peak wavelength at 100 cd m⁻². ^{b)} Full width at half maximum of the spectra given in wavelength. ^{c)} Turn-on voltage at 1 cd m⁻². ^{d)} Maximum luminance. ^{e)} Maximum current efficiency. ^{f)} Maximum power efficiency. ^{g)} Maximum external quantum efficiency, and values at 100 and 1000 cd m⁻², respectively. ^{h)} Value taken at 100 cd m⁻².

Table S8. Summary of the EL data of the Spiro-3TCzBN, DPh-3TCzBN and DMe-3TCzBN-based devices with sensitizer.

emitter	$\lambda_{\text{em}}^{\text{a})}$ [nm]	FWHM ^{b)} [nm/eV]	$V_{\text{on}}^{\text{c})}$ [V]	$L_{\text{max}}^{\text{d})}$ [cd m ⁻²]	CE _{max} ^{e)} [cd A ⁻¹]	PE _{max} ^{f)} [lm W ⁻¹]	EQE ^{g)} [%]	CIE ^{h)} (x, y)
Spiro-3TCzBN	560	53/0.18	2.7	142450	129.6	136.5	35.3/35.1/34.1	(0.444, 0.546)
DPh-3TCzBN	568	58/0.21	2.7	151140	109.7	116.3	35.4/34.6/30.0	(0.471, 0.519)
DMe-3TCzBN	572	56/0.21	2.7	146590	115.5	127.8	34.8/33.4/26.9	(0.493, 0.491)

^{a)} EL peak wavelength at 100 cd m⁻². ^{b)} Full width at half maximum of the spectra given in wavelength. ^{c)} Turn-on voltage at 1 cd m⁻². ^{d)} Maximum luminance. ^{e)} Maximum current efficiency. ^{f)} Maximum power efficiency. ^{g)} Maximum external quantum efficiency, and values at 100 and 1000 cd m⁻², respectively. ^{h)} Value taken at 100 cd m⁻².

Table S9. Summary of EL data of representative CP-MR-TADF emitters.

Compound	Photoluminescence		Electroluminescence		Ref.
	λ_{PL} (nm) ^{a)}	FWHM(nm)	$g_{EL}(10^{-3})$	EQE(%)	
R/S-BN-MeIAc	497	30	+0.27/-0.29	37.2/36.1	[10]
R/S-Spiro-BNCz	528	42	+0.81/-1.0	34.2	[11]
R/S-p-Spiro- DtBuCzB	491	25	+0.322/-0.349	29.6	[12]
R/S-m-Spiro- DtBuCzB	502	33	+0.785/-0.747	33.8	[12]
R/S-NBOPO	462	25	+0.702/-0.780	16.4	[13]
R/S-NBNPO	498	24	+1.46/-1.40	28.3	[13]
R/S-OBN-2CN-BN	493	22	+1.43/-1.27	29.4	[14]
R/S-OBN-4CN-BN	500	27	+0.46/-0.48	24.5	[14]
R/S-DOBn	453	21	-0.9/+0.9	23.9	[15]
R/S-DOBNT	459	21	-1.0/+0.9	25.6	[15]
R/S-S-AX-BN	489	21	+3.3/-3.2	33.5	[16]
R/S-SO ₂ -AX-BN	495	20	+2.2/-2.1	31.5	[16]
R/S-BDBF-BNO	460	27	+1.5/-1.3	32.1	[17]
R/S-BDBT-BNO	460	27	+1.6/-1.4	35.7	[17]
R/S-BDBF-BOH	458	27	-0.59/+0.59	29.5	[18]
R/S-BDBT-BOH	459	27	-1.1/+1.2	30.1	[18]
R/S-BACzBO	482	—	+3.5/-3.9	37.4/36.6	[19]
R/S-BA23CzBN	490	27	+0.31/-0.22	36.6/34.6	[20]
R/S-BA34CzBN	515	34	+1.1/-1.2	36.0/36.1	[20]
R/S-DtCzB-OBN	491	22	+0.34/-0.311	30.0	[21]

<i>R/S</i> -DtCzB-BN	494	22	+0.799/-0.819	33.9	[21]
<i>R/S</i> -Czp-tBuCzB	478	23	+1.54/-1.48	32.1	[22]
<i>R/S</i> -Czp-POAB	498	36	+1.3/-1.25	28.7	[22]
<i>R/S</i> -PCP-DiKTa	469	44	–	25.7	[23]
<i>R/S</i> -Czp-DiKTa	505	66	–	27.8	[23]
<i>P, P/M, M-1a</i>	662	38	–	28.1	[24]
<i>P, P/M, M-1b</i>	692	38	–	27.6	[24]
<i>P, P/M, M-RBNN</i>	617	38	-1.77/+1.91	34.4/36.6	[25]
<i>P/M-o[B-N]₂N₂</i>	542	21	+0.77/-0.67	25.1	[26]
<i>P/M-BN4</i>	500	43	+3.7/-3.1	20.6/19.0	[27]
<i>P/M-BN5</i>	497	44	+1.9/-1.6	22.0/26.5	[27]
<i>P/M-helicene-BN</i>	525	48	+1.2/-2.2	31.5/30.7	[28]
<i>P, P/M, M-3-C2</i>	543	23	–	–	[29]
<i>P, P/M, M-4-C1</i>	520	28	–	–	[29]
<i>P/M-BN-Py</i>	527	35	-0.437/+0.435	30.6/29.2	[30]
<i>P/M-BN-TPICz</i>	531	36	+0.649/-0.774	32.0	[31]
<i>P/M- BN[9]H</i>	578	47	-6.2/+4.9	35.4/35.5	[31]
<i>P/M-DB-O</i>	443	24	-2.2/+2.2	27.5	[32]
<i>P/M-DB-S</i>	444	23	-2.6/+2.6	29.3	[32]
<i>P/M-QAO-PhCz</i>	461	29	+1.5/-1.5	14.0	[33]
<i>P/M-QPO-PhCz</i>	446	33	-1.1/+1.6	10.6	[34]
<i>P/M-HeI-DiDiKTa</i>	473	44	–	–	[35]

8. References

- 1 A. D. Becke, *J. Chem. Phys.*, 1993, **98**, 5648.
- 2 C. Lee, W. Yang, R. G. Parr, *Phys. Rev. B*, 1988, **37**, 785.
- 3 R. Krishnan, J. S. Binkley, R. Seeger, J. Pople, *J. Chem. Phys.*, 1980, **72**, 650.
- 4 S. Grimme, J. Antony, S. Ehrlich, H. Krieg, *J. Chem. Phys.*, 2010, **132**, 154104.
- 5 Gaussian 09, Revision D.01, M. J. Frisch, G. W. Trucks, H. B. Schlegel, G. E. Scuseria, M. A. Robb, J. R. Cheeseman, G. Scalmani, V. Barone, B. Mennucci, G. A. Petersson, H. Nakatsuji, M. Caricato, X. Li, H. P. Hratchian, A. F. Izmaylov, J. Bloino, G. Zheng, J. L. Sonnenberg, M. Hada, M. Ehara, K. Toyota, R. Fukuda, J. Hasegawa, M. Ishida, T. Nakajima, Y. Honda, O. Kitao, H. Nakai, T. Vreven, J. A. Montgomery, Jr., J. E. Peralta, F. Ogliaro, M. Bearpark, J. J. Heyd, E. Brothers, K. N. Kudin, V. N. Staroverov, T. Keith, R. Kobayashi, J. Normand, K. Raghavachari, A. Rendell, J. C. Burant, S. S. Iyengar, J. Tomasi, M. Cossi, N. Rega, J. M. Millam, M. Klene, J. E. Knox, J. B. Cross, V. Bakken, C. Adamo, J. Jaramillo, R. Gomperts, R. E. Stratmann, O. Yazyev, A. J. Austin, R. Cammi, C. Pomelli, J. W. Ochterski, R. L. Martin, K. Morokuma, V. Zakrzewski, G. A. Voth, P. Salvador, J. J. Dannenberg, S. Dapprich, A. D. Daniels, O. Farkas, J. B. Foresman, J. V. Ortiz, J. Cioslowski, and D. J. Fox, Gaussian, Inc., Wallingford CT, 2013.
- 6 Humphrey, W. Dalke, A. Schulten, K. VMD: visual molecular dynamics. *J. Mol. Graph.*, 1996, **14**, 33.
- 7 Q. Zhang, H. Kuwabara, W. J. Potscavage, S. Huang, Y. Hatae, T. Shibata, C. Adachi, *J. Am. Chem. Soc.*, 2014, **136**, 18070.
- 8 Q. Zhang, B. Li, S. Huang, H. Nomura, H. Tanaka, C. Adachi, *Nat. Photonics*, 2014, **8**, 326.
- 9 T.-L. Wu, M.-J. Huang, C.-C. Lin, P.-Y. Huang, T.-Y. Chou, R.-W. Chen-Cheng, H.-W. Lin, R.-S. Liu, C.-H. Cheng, *Nat. Photonics*, 2018, **12**, 235.
- 10 Y. Yang, N. Li, J. Miao, X. Cao, A. Ying, K. Pan, X. Lv, F. Ni, Z. Huang, S. Gong, C. Yang, *Angew. Chem. Int. Ed.*, 2022, **61**, e202202227.
- 11 X. Luo, S. Song, X. Wu, C. Yip, S. Cai, Y. Zheng, *Aggregate*, 2024, **5**, e445.

- 12 S. Song, X. Han, Z. Huo, C. Yip, X. Hong, M. Ding, Y. Zheng, *Sci. China Chem.*, 2024, **67**, 2257.
- 13 Y. Wang, Z. Lv, Z. Chen, S. Xing, Z. Huo, X. Hong, L. Yuan, W. Li, Y. Zheng, *Mater. Horiz.*, 2024, **11**, 4722.
- 14 Y. Xu, Q. Wang, X. Cai, C. Li, Y. Wang, *Adv. Mater.*, 2021, **33**, 2100652.
- 15 Z.-P. Yan, L. Yuan, Y. Zhang, M.-X. Mao, X.-J. Liao, H.-X. Ni, Z.-H. Wang, Z. An, Y.-X. Zheng, J.-L. Zuo, *Adv. Mater.*, 2022, **34**, 2204253.
- 16 X. Wang, S. Xing, X. Xiao, L. Yuan, Z. Hou, Y. Zheng, *Adv. Funct. Mater.*, 2024, **34**, 2412044.
- 17 L. Yuan, Y. Yang, Z. Yan, J. Hu, D. Mao, H. Ni, Y. Zheng, *Adv. Funct. Mater.*, 2024, **34**, 2403803.
- 18 L. Yuan, J. Xu, Z. Yan, Y. Yang, D. Mao, J. Hu, H. Ni, C. Li, J. Zuo, Y. Zheng, *Angew. Chem. Int. Ed.*, 2024, **63**, e202407277.
- 19 X. Yin, H. Huang, N. Li, W. Li, X. Mo, M. Huang, G. Chen, J. Miao, C. Yang, *Mater. Horiz.*, 2024, **11**, 1752.
- 20 H. Huang, N. Li, W. Li, X. Mo, X. Cao, J. Miao, X. Yin, C. Yang, *Adv. Funct. Mater.*, 2024, **34**, 2403191
- 21 S. Xing, X. Zhong, X. Liao, Y. Wang, L. Yuan, H. Ni, Y. Zheng, *Adv. Opt. Mater.*, 2024, **12**, 2400685.
- 22 X. Liao, D. Pu, L. Yuan, J. Tong, S. Xing, Z. Tu, J. Zuo, W. Zheng, Y. Zheng, *Angew. Chem. Int. Ed.*, 2023, **62**, e202217045.
- 23 Y. Xu, H. Hafeez, J. Seibert, S. Wu, J. Ortiz, J. Crassous, S. Bräse, I. Samuel, E. Zysman-Colman, *Adv. Funct. Mater.*, 2024, **34**, 2402036.
- 24 J. Li , X. Chen, Y. Guo, X. Wang, A. Sue, X. Cao, X. Wang, *J. Am. Chem. Soc.*, 2021, **143**, 17958.
- 25 G. Meng, J. Zhou, X. Han, W. Zhao, Y. Zhang, M. Li, C. Chen, D. Zhang, L. Duan, *Adv. Mater.*, 2024, **36**, 2307420.
- 26 Yuan L., Z. Tu, J. Xu, H. Ni, Z. Mao, W. Xu, Y. Zheng, *Sci. China Chem.*, 2023, **66**, 2612.
- 27 X. Wu, J. Huang, B. Su, S. Wang, L. Yuan, W. Zheng, H. Zhang, Y. Zheng, W. Zhu , P. Chou, *Adv. Mater.*, 2022, **34**, E2105080.
- 28 Yang W, Li N, Miao J, Zhan L, Gong S, Huang Z, Yang C. CCS Chem., 2022, 4, 3463.

- 29 F. Zhang, F. Rauch, A. Swain, T. Marder, P. Ravat, *Angew. Chem. Int. Ed.*, 2023, **62**, e202218965.
- 30 Q. Wang, L. Yuan, C. Qu, T. Huang, X. Song, Y. Xu, Y.-X. Zheng, Y. Wang, *Adv. Mater.*, 2023, **35**, 2305125.
- 31 T. Huang , L. Yuan, X. Lu, Y. Qu, C. Qu, Y. Xu, Y. Zheng, Y. Wang, *Chem. Sci.*, 2024, **15**, 15170.
- 32 Z. Ye, H. Wu, Y. Xu, T. Hua, G. Chen, Z. Chen, X. Yin, M. Huang, K. Xu, X. Song, Z. Huang, X. Lv, J. Miao, X. Cao, C. Yang, *Adv. Mater.*, 2024, **36**, 2308314.
- 33 S. Yang, S. Zou, F. Kong, X. Liao, Y. Qu, Z. Feng, Y. Zheng, Z. Jiang, L. Liao, *Chem. Commun.*, 2021, **57**, 11041.
- 34 S. Yang, Q. Tian, X. Liao, Z. Wu, W. Shen, Y. Yu, Z. Feng, Y. Zheng, Z. Jiang, L. Liao, *J. Mater. Chem. C*, 2022, **10**, 4393.
- 35 J. dos Santos, D. Sun, J. Moreno-Naranjo, D. Hall, F. Zinna, S. Ryan, W. Shi, T. Matulaitis, D. Cordes, A. Slawin, D. Beljonne, S. Warriner, Y. Olivier, M. Fuchter, E. Zysman-Colman, *J. Mater. Chem. C*, 2022, **10**, 4861.